Published in final edited form as:

Curr Biol. 2023 January 09; 33(1): 58–74.e5. doi:10.1016/j.cub.2022.11.038.

Connections between sister and non-sister telomeres of segregating chromatids maintain euploidy

Brandt Warecki[*,1], **Ian Bast**[1], **Matthew Tajima**[1], **William Sullivan**[1]

[1]Department of Molecular, Cell, and Developmental Biology; University of California, Santa Cruz; 1156 High Street, Santa Cruz, CA, 95064, USA

Summary

The complete separation of sister chromatids during anaphase is a fundamental requirement for successful mitosis. Therefore, divisions with either persistent DNA-based connections or lagging chromosome fragments threaten aneuploidy if unresolved. Here, we demonstrate the existence of an anaphase mechanism present in normally dividing cells in which pervasive connections between telomeres of segregating chromosomes aid in rescuing lagging chromosome fragments. We observe that in a large proportion of *Drosophila melanogaster* neuronal stem cell divisions, early anaphase sister and non-sister chromatids remain connected by thin telomeric DNA threads. Normally, these threads are resolved in mid-to-late anaphase via a spatial mechanism. However, we find that the presence of a nearby unrepaired DNA break recruits histones, BubR1 kinase, Polo Kinase, Aurora B kinase, and BAF to the telomeric thread of the broken chromosome, stabilizing it. Stabilized connections then aid lagging chromosome rescue. These results suggest a model in which pervasive anaphase telomere-telomere connections that are normally resolved quickly can instead be stabilized to retain wayward chromosome fragments. Thus, the liability of persistent anaphase inter-chromosomal connections in normal divisions may be offset by their ability to maintain euploidy in the face of chromosome damage and genome loss.

Graphical Abstract

[*]Correspondence and lead contact: bwarecki@ucsc.edu.

Author contributions

Conceptualization: B.W. and W.S.; Methodology: B.W. and W.S.; Validation: B.W., I.B., and M.T.; Formal Analysis: B.W., I.B., and M.T.; Investigation: B.W., I.B., and M.T.; Writing – Original Draft: B.W. and W.S.; Writing – Reviewing & Editing: B.W. and W.S.; Visualization: B.W. and W.S.; Supervision: B.W. and W.S.; Funding Acquisition: W.S.

Inclusion and diversity

While citing references scientifically relevant for this work, we also actively worked to promote gender balance in our reference list.

Declaration of interests

The authors declare no competing interests.

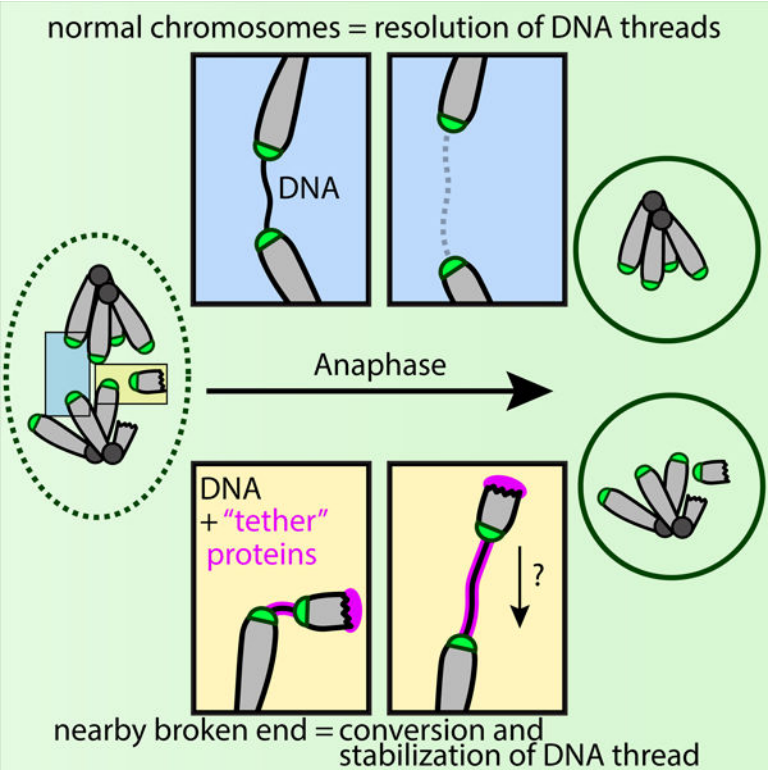

eTOC Blurb

Warecki *et al.* show that prevalent DNA threads connecting telomeres of anaphase chromosomes are stabilized upon chromosome breakage and recruit proteins that retain the resulting fragment. These findings suggest that otherwise dangerous connections between anaphase chromosomes can be beneficial by preventing potential loss of genetic material.

Keywords

genome integrity; cancer; euploidy; aneuploidy; ultrafine bridge; DNA tether; mitosis; acentric; telomeres; neuroblast

Introduction

Successful mitosis creates two genetically identical daughter cells. This is primarily achieved at the metaphase-to-anaphase transition, when sister chromatids separate and segregate to opposing poles. Incomplete separation of chromatids can result in daughter cells with either missing or extra genetic material. For example, during the breakage-fusion-bridge cycle—when two distinct chromosomes fuse, form a bridge in anaphase, and break—daughter cells have non-identical genomes if the break occurs asymmetrically [1]. Multiple rounds of these cycles result in extensive aneuploidy characteristic of cancer [2–6]. Similarly, catastrophic aneuploidy results from cells that either mis-segregate chromosomes or fail to segregate chromosome fragments [7–9].

To minimize such deleterious outcomes, evolved mechanisms promote entry into anaphase once separation of the duplicated genome is likely to be complete. For instance, the spindle assembly and DNA damage checkpoints prevent entry into anaphase when chromosomes are improperly attached to the mitotic spindle, incompletely replicated, or damaged [10–12]. Additionally, the ends of chromosomes are capped by telomeres, which prevent fusion between separate chromosomes and bridging during anaphase [13,14]. These mechanisms are highly conserved, underscoring their critical role in maintaining genomic integrity.

However, eukaryotic cells can still enter anaphase with lingering attachments between segregating chromatids or with unrepaired DNA breaks. Anaphase inter-chromosomal connections have been observed in yeast [15,16], mammalian [17–21], and insect [22–24] divisions and may be the norm in most dividing animal cells [25]. For example, anaphase chromosomes can remain attached via ultrafine bridges. Ultrafine bridges are DNA strands that link separating sister chromatids and are likely present in most divisions[18,26]. While centromere-based ultrafine bridges are most common, ultrafine bridges can originate from multiple locations along a chromosome, including at telomeres [26]. Although ultrafine bridges may contribute to sister chromatid tension and telomere maintenance [27,28], their functional significance, if any, remains unclear. Mutants in proteins that localize to and resolve ultrafine bridges--such as BLM, PICH, Rif1, or TopBP1--cause chromosome instability, aneuploidy, cell death, and potentially cancer [15,17,18,29,30]. Thus, ultrafine bridges and other anaphase inter-chromosomal connections threaten the genomic integrity of dividing cells, and their resolution is required for euploidy [15,26,31–33].

Additionally, entering anaphase with chromosome fragments, as observed in some cancers and cells lacking DNA damage checkpoints [34,35], can be particularly dangerous for dividing cells. If a lagging fragment is excluded from daughter nuclei, it forms a micronucleus [8]. Micronuclei undergo extensive DNA damage altering gene copy number and driving aneuploidy [9,36]. To maintain euploidy in response to division with broken chromosomes, some cells activate mechanisms that aid integration of chromosome fragments into daughter nuclei [37–40]. For example, in *Drosophila* neuroblasts, protein-coated DNA “tethers” form to specifically connect the broken ends of chromosome fragments to segregated nuclei, resulting in efficient rescue of the fragments [23,41–43]. The proteins localized to this tether—histones, BubR1, Bub3, Fizzy, Polo, Aurora B, INCENP, and BAF [23,43,44]—are recruited to the tether by recognition of the double-stranded DNA break [45]. Similar mechanisms retain broken chromosomes in *Drosophila* papillar cells [35,46] and cultured human cells [20,47]. Although the proteins involved in retention differ, each mechanism depends upon recognizing DNA damage. Failure to enact these mechanisms results in micronuclei formation, aneuploidy, and cell death [23,35,41,43,46].

Understanding of the mechanisms that act in anaphase to promote euploidy in the face of such division abnormalities remains limited. Here, we find evidence for a mechanism acting in normally dividing *Drosophila* neuroblast cells in which the first form of division errors (persistent inter-chromosomal connections) rescues the second (chromosome fragments). We observe: 1) early anaphase chromosomes separating to opposing poles remain connected by thin DNA threads predominantly originating from telomeric regions; 2) in the absence of a double-stranded DNA break, these connections are resolved in mid-to-late anaphase

as the ends of chromosomes move apart; 3) the presence of a nearby double-stranded DNA break can stabilize these telomere connections; and 4) stabilized connections may aid broken chromosome segregation and incorporation into daughter nuclei. Collectively, these results suggest a novel mechanism in which telomeric connections between segregating chromosomes during early anaphase are tolerated and may allow for efficient retention of lagging chromosomes.

Results

DNA threads connect chromosomes segregating to opposing poles in early anaphase

Given the prevalence of anaphase inter-chromosomal connections in other species [25,26], we wished to determine if similar connections linked the segregating chromosomes of *Drosophila* neuroblasts. Therefore, we fixed neuroblasts derived from control *y1v1* 3rd instar larvae and stained DNA with the dye 4’6-diamidino-2-phenylindole (DAPI). We performed Airyscan super-resolution imaging on neuroblasts fixed in early-to-late anaphase and focused on detecting the presence of DNA threads connecting segregating sister chromatids.

Anaphase chromosome segregation appeared normal in all neuroblasts imaged, with no chromosome bridges present in any division (N=53; Figure 1, left panels). However, post-acquisition adjustment of brightness and contrast revealed the existence of DAPI-stained threads connecting chromosomes segregating to opposing poles in a substantial proportion of anaphases (Figure 1, middle and right panels, arrows). Overall, we observed inter-chromosomal threads in 38% of anaphases imaged (Figure 1A-B). Notably, the ends of chromosome arms connected by threads were directly facing one another (Figure 1A-B, arrowheads), suggesting the ends of these chromosomes may be physically connected under tension.

We next classified the observed threads into two categories based on the strength of their DAPI signals. Complete, uninterrupted (++) threads had continuous DAPI staining stretching from the end of one chromosome to the end of an opposing chromosome and were observed in 14% of anaphases (Figure 1A). Complete, interrupted (+) threads had intermittent DAPI staining stretching from the end of one chromosome to the end of an opposing chromosome and were observed in 24% of anaphases (Figure 1B).

The 62% of divisions scored as not containing threads fell into two categories. Stretched/erstwhile threads (−) showed limited evidence of possible threads, with intermittent DAPI staining emerging from the end of one chromosome towards the end of an opposing chromosome (Figure 1C). This classification could include 1) threads that had become highly stretched to a point beyond our detection, and/or 2) threads that had recently been resolved. As we cannot distinguish between these possibilities, we classified these divisions as not containing threads. However, this classification may contain threads we cannot visualize. We observed this classification in 17% of anaphases. Additionaly, we detected no evidence (−−) of inter-chromosomal threads in 45% of anaphases imaged (Figure 1D).

To determine if inter-chromosomal threads were more likely to be present early in anaphase, we binned each division based on its stage (see STAR Methods; Figure 1E) and compared the strengths of threads observed at each stage (Figure 1E'). This revealed inter-chromosomal threads were present in 78% of early anaphases (N=9), 39% of mid anaphases (N=28), and 12% of late anaphases (N=16). These differences were statistically significant (two-sided Fisher's exact test p=0.005). Furthermore, while we observed our strongest classification of thread (++) in 67% of early anaphases, we detected ++ threads in 4% and 0% of mid and late anaphases respectively (two-sided Fisher's exact test p<0.001). Additionally, we observed a considerable percentage (36%) of the stretched/erstwhile (−) classification of threads in mid anaphase, suggesting threads may frequently become highly stretched and/or resolved during this time. Thus, inter-chromosomal threads are common in early anaphase but are mostly resolved by late anaphase.

Given threads were visible soon after chromosome ends separated in early anaphase, we wondered if threads may exist before anaphase. We analyzed neuroblasts fixed in prometaphase and metaphase. While limited spatial separation of chromosomes during these stages prevented accurate quantification of the number of threads, we observed several pre-anaphase cells (6/14) with apparent DAPI-stained connections between separate chromosomes (Figure S1A, arrow). We observed DAPI-stained threads between chromosome arms as well as chromosome ends, including apparent connections between the ends of non-homologous chromosomes. The presence of DNA threads in early mitotic cells suggests some threads may form before anaphase.

To demonstrate the observed inter-chromosomal threads are not an artifact of DAPI staining, we fixed and stained neuroblasts with the nucleic acid dye propidium iodide (PI) (Figure 1F). Whereas DAPI binds the minor groove of DNA, PI intercalates between the bases. As PI detects both DNA and RNA, we performed an RNA digestion step before PI staining. As with DAPI-stained neuroblasts, we observed inter-chromosomal threads (arrow) connecting the ends of chromosomes segregating to opposing poles (arrowheads) in 30% (N=33) of PI-stained anaphase neuroblasts (Figure 1F). Thus, inter-chromosomal threads are DNA-based and detectable by dyes that bind DNA through different mechanisms.

Next, to examine how inter-chromosomal connections affect chromosome dynamics, we live imaged dividing *y1v1* neuroblasts expressing histone H2Av-RFP, enabling chromosome visualization. In 9/30 divisions, a segregating chromosome arm seemingly moved backward towards the opposite nucleus after having already begun poleward motion (Figure S1B, arrows). The affected chromosome arm then rejoined the other chromosomes segregating poleward. These movements are consistent with a persistent physical connection between the ends of chromosomes segregating to opposing poles, possibly due to unresolved inter-chromosomal threads. Alternatively, these movements could be caused by merotelic attachments pulling the affected chromatids to both poles. We did not detect any histone signal between chromosomes segregating to opposing nuclei (0/30 divisions), suggesting anaphase inter-chromosomal threads consist of DNA but not histones.

DNA threads originate from or near capped telomeres

To determine where on chromosomes inter-chromosomal threads form, we analyzed the locations from which inter-chromosomal DNA threads originated. We mainly observed inter-chromosomal DNA threads originating from chromosome ends (65%, N=66) (Figure 1G, arrow) or near chromosome ends (within 5% of the length of the chromosome arm) (27%, N=66) (Figure 1G, arrowhead). We did not detect any threads obviously emanating from the arms of chromosomes, although 5/66 (8%) of thread ends had indeterminant origins hidden in the mass of chromatin.

To test if threads were originating from capped telomeres, we fixed neuroblasts expressing HOAP-GFP, a telomere capping protein [48], and stained with DAPI and antibodies against GFP (Figure 1H-H'). We observed numerous threads (arrows) emerging directly from or adjacent to HOAP-capped telomeres (arrowheads indicate thread origins) (Figure 1H). Rarely, we observed threads that seemingly emerged from areas with no HOAP (Figure 1H). The average distance between the thread origin and the HOAP-capped telomere was 0.25 μm, with multiple origins closer than the z-pixel width used in our imaging (Figure 1H'). Collectively, these data suggest inter-chromosomal DNA threads are not specific to a particular locus. However, their existence during anaphase seems mainly limited to areas at or near capped telomeres.

DNA threads may depend upon the activity of the single-stranded DNA binding protein RpA-70

We reasoned DNA threads between separating sister chromatids may involve single-stranded DNA during their formation, be it DNA replication, homologous recombination, and/or DNA repair. Therefore, we analyzed anaphases in which the single-stranded DNA binding protein RpA-70 [49] (RPA1 in humans) was reduced by expressing RNA interference (RNAi) under control of transgenic Upstream Activating Sequences (UAS).

Driving UAS-RpA-70-RNAi in neuroblasts by expressing elav-Gal4 resulted in small larval brains with few mitotic cells. The mitotic cells we could observe often underwent aberrant divisions (Figure S1C), likely due to RpA-70's role in multiple essential processes [50]. In the rare relatively normal mitoses, cells were fixed in late anaphase with no detectable threads (Figure S1C). The lack of mitotic cells upon strong RpA-70 reduction precluded in depth analysis of RpA-70 involvement in thread formation. However, larvae lacking Gal4 still exhibited small brains at low frequency, suggesting "leaky" RpA-70-RNAi expression in the absence of Gal4. These brains contained more mitotic cells. Therefore, we analyzed mitotic neuroblasts expressing low levels of UAS-RpA-70-RNAi in the absence of Gal4.

In total, we observed threads in 49% (N=75) of control and 37% (N=73) of UAS-RpA-70-RNAi neuroblasts fixed concurrently (Figure S1D). As threads are largely undetectable by late anaphase (Figure 1E'), we focused on neuroblasts fixed in early and mid anaphase (Figure S1E). We observed a moderate, significant reduction in the percentage of threads in early and mid anaphase UAS-RpA-70-RNAi neuroblasts (*y1v1*=69%, N=49; UAS-RpA-70-RNAi=48%, N=52; two-sided Fisher's exact test p=0.04). Additionally, the number of threads per division was slightly but significantly reduced in UAS-RpA-70-RNAi

neuroblasts (*y1v1*=1.2 threads/division; UAS-RpA-70-RNAi=0.79 threads/division; Mann-Whitney test p=0.038) (Figure S1F), suggesting threads may depend upon RpA-70 activity. However, further research is required to test if RpA-70 indeed contributes to anaphase DNA thread formation and/or stability.

Inter-chromosomal DNA threads are mainly resolved by a spatial mechanism

Despite the presence of inter-chromosomal DNA threads in a large proportion of early divisions, *y1v1* flies are healthy, suggesting the observed DNA threads are efficiently resolved during mitosis. The dramatic reduction in detectable DNA threads in late anaphase (Figure 1E) is consistent with resolution of anaphase DNA threads before mitotic exit.

Inter-chromosomal DNA threads could be resolved by a spatial or temporal mechanism. To distinguish between these possibilities, we fixed and DAPI-stained neuroblasts containing extra-long chromosome arms with ends that would be near to one another even during mid-to-late anaphase. We imaged neuroblasts containing either the In(3LR) chromosome, in which an inversion of the 3rd chromosome results in an elongated chromosome arm [51], or the C(2)EN chromosome, in which both homologs of the 2nd chromosome are on a single centromere [52] (Figure 2A). As with normal-length chromosomes from previously imaged *y1v1* neuroblasts, we observed threads connecting the telomeres of extra-long sister chromatids segregating to opposing poles in both In(3LR) and C(2)EN-bearing neuroblasts (Figure 2B; *y1v1*=38%, N=53; In(3LR)=55%, N=49; C(2)EN=34%, N=47).

With a temporal mechanism of thread resolution, DNA threads should be present only in early anaphase, regardless of the cell containing extra-long chromosomes (Figure 2C). In contrast, a spatial mechanism of resolution predicts DNA threads should also be present in mid-to-late anaphase for cells bearing extra-long chromosomes. This is because the distance between the ends of extra-long chromatids later in anaphase is comparable to the distance between the ends of normal-length chromatids earlier in anaphase (Figure 2C).

Therefore, we compared the percentages of threads in mid and late anaphase between neuroblasts with extra-long or normal-length chromosomes. Consistent with a spatial mechanism of resolution, we detected inter-chromosomal threads in mid anaphase neuroblasts containing either extra-long In(3LR) or C(2)EN chromosomes at significantly higher rates than in mid anaphase *y1v1* neuroblasts with normal-length chromosomes (*y1v1*=39%, N=28; In(3LR)=72%, N=32; C(2)EN=50%, N=22) (Figure 2D; two-sided Fisher's exact test p=0.04). Similarly, the frequencies of the strongest classification of threads (++) were significantly increased when mid anaphase neuroblasts contained extra-long chromosomes (*y1v1*=4%, N=28; In(3LR)=41%, N=32; C(2)EN=32%, N=22; two-sided Fisher's exact test p=0.002). By late anaphase, the difference in frequencies of threads was no longer statistically significant (two-sided Fisher's exact test p=0.77), although the frequencies of threads in In(3LR)- and (C(2)EN-bearing neuroblasts were still increased compared to *y1v1* controls (*y1v1*=12%, N=16; In(3LR)=24%, N=17; C(2)EN=20%, N=25). The persistence of threads in neuroblasts containing extra-long chromosomes indicates inter-chromosomal threads are mainly resolved by a spatial, not temporal, mechanism.

Consistent with spatial resolution, we observed similar distances between the ends of connected chromosomes in *y1v1*, In(3LR)-, and C(2)EN-bearing neuroblasts (Figure 2E). This suggests the main determinant for the presence of a thread is the physical distance between chromosome ends. However, while these distributions were not statistically significant (Kruskal-Wallis test p=0.23), we were unable to detect >2 μm threads in C(2)EN-bearing neuroblasts despite detecting them in *y1v1* control and In(3LR)-bearing neuroblasts (Figure 2E). Anaphase C(2)EN chromosome arms are slightly more elongated than In(3LR) chromosome arms (Figure S2A-B, [51]). Therefore, there may be an upper temporal limit on thread persistence, perhaps due to cytokinesis.

Nevertheless, for all genotypes combined, we found the stronger classification of complete, uninterrupted (++) threads were generally observed when the distances between connected chromosome ends were <1 μm (Figure 2E'). The weaker classification (+) was mainly observed when the distances between connected chromosome ends were >1 μm (Figure 2E'). These results suggest inter-chromosomal DNA threads stretch and then resolve as chromosome ends move apart.

DNA threads between the ends of extra-long chromosomes may recruit histones

Our inability to detect histones between the ends of segregating normal-length chromosomes (Figure S1B) may be because DNA threads are highly stretched. As the ends of extra-long chromosomes remain near one another during early and mid anaphase, threads connecting extra-long chromosomes may be under less tension and more suitable for histone recruitment. Therefore, we live imaged neuroblasts bearing the extra-long In(3LR) chromosome and expressing H2Av-RFP.

While we were unable to detect histones linking the ends of separating extra-long chromosomes in most divisions (Figure S2C-C'), in rare cases, we observed faint H2Av-RFP signal connecting the ends of extra-long chromosomes that had just separated (Figure S2D-E', arrows). These results suggest DNA threads under less tension can recruit histones, albeit infrequently. We observed histone-coated threads in 3/28 divisions imaged (Figure S2F).

Separated extra-long sister chromatids exhibit coordinated movements

Consistent with a physical connection linking sister chromatids, the ends of extra-long chromosomes appeared to exhibit coordinated movements as if one end physically pulled on the other (Figure S2C timepoints 40–300; S2D timepoints 320–480; S2E timepoints 20–350). We observed coordinated movements in 10/28 divisions (Figure S2F), including in all divisions in which we could detect histone-coated threads. Chromosomes exhibiting coordinated movement should have similar angles between the chromosome ends and the division axis (Figure S2G). We measured the angles between the long chromosome ends and the division axes for 200 seconds following chromosome end separation (Figure S2G'). For a division exhibiting uncoordinated movement (Figure S2G', dashed lines), the measured angles behaved independently. However, for a division exhibiting coordinated movement between chromosome ends (Figure S2G', solid lines), the measured angles tracked one

another. These coordinated movements suggest DNA threads may transmit force between chromosomes separating to opposing poles.

DNA threads connect the telomeres of segregated chromosomes to sister and non-sister telomeres of lagging chromosomes and chromosome fragments

Given the spatial resolution of threads, we wondered if lagging chromosomes and chromosome fragments could remain connected to nearby segregated chromosomes. Similar to DNA-protein tethers that link the broken ends of chromosome fragments [23,47], persistent telomere-telomere connections may secure lagging chromosomes to segregated chromosomes. Therefore, we generated lagging chromosomes in neuroblasts by creating acentric chromosomes with intact telomeres and no centromeres and asked if we could detect threads connecting these lagging acentrics to segregated centric chromosomes.

To generate acentric lagging whole chromosomes, we expressed the recombinase FLP in neuroblasts containing transgenic chromosomes with inverted FRTs [14]. In this system, FLP-mediated recombination of the inverted FRTs results in a dicentric chromosome and an unbroken acentric, analogous to a whole chromosome that failed to attach to the spindle (Figure 3A). Threads connected the unbroken acentrics to the centric chromosomes in 34% of divisions imaged (N=44), 18% in total from the strongest classification of thread (++; complete, uninterrupted) (Figure 3B, arrows; Figure 3F). Thus, persistent DNA threads link the telomeres of lagging chromosomes to the telomeres of segregated chromosomes. Additionally, because generation of the unbroken acentric results in sister telomeres being rearranged onto the same DNA molecule (Figure 3A), the observed threads connecting unbroken acentrics to segregated chromosomes demonstrate that DNA threads connect non-sister as well as sister telomeres.

We next asked if telomere-telomere threads persist on lagging chromosome fragments resulting from chromosome breakage. We generated broken acentric fragments by expressing the endonuclease I-CreI (Figure 3C), which cuts at the base of the sex chromosomes [53] to create 4 distinct fragments (labeled 1–4 in Figure 3D-E). We observed DNA threads connecting acentric fragments in 87% (N=54) of analyzed neuroblasts, 70% from the strongest classification of thread (++, complete, uninterrupted) (Figure 3D, arrow; Figure 3F). Some observed threads correspond to the DNA component of protein-coated “tethers” that link the broken end of the acentric to the broken end of the centric fragment [23] (from here on, tethers=DNA threads + “tether” proteins). However, we also observed divisions in which DNA threads emanated from both ends of broken acentrics simultaneously (Figure 3E). In these cases, one thread connected the acentric to the nearby segregated chromosomes (Figure 3E, arrow) while the second thread connected the other end of the acentric to either another acentric (Figure 3E, arrowhead) or chromosomes segregated to the opposite pole. Because one end of the broken acentric is the telomere end, DNA threads emanating from both ends of acentrics demonstrate telomere-telomere connections persist after a chromosome is broken. Strong DNA threads between acentrics segregating to opposing nuclei in *Drosophila* neuroblasts were reminiscent of inter-chromosomal DNA connections we could detect between lagging chromosomes in human cancer cells (Figure S3A-B).

These results indicate lagging chromosomes remain connected to segregated chromosomes via telomere-telomere DNA connections. Additionally, the significantly increased frequency (unbroken acentrics=34%; broken acentrics=87%; two-sided Fisher's exact test $p<0.001$) and strength (unbroken acentrics=18% ++ threads; broken acentrics=70% ++ threads; two-sided Fisher's exact test $p<0.001$) of threads connected to broken acentrics compared to those connected to unbroken acentrics (Figure 3F) suggests chromosome breakage is correlated with more robust threads. Consistent with this view, threads connecting to broken acentrics were quantifiably brighter than threads connecting unbroken acentrics (Figure 3G; Mann-Whtiney test $p<0.001$). Increased thread frequency and strength are likely due to the formation of protein-coated tethers upon recognition of the broken end [23,45].

Histones are recruited to DNA threads emanating from sister and non-sister telomeres of broken acentrics

Given our observation of frequent DNA threads emanating from both ends of broken acentrics, we wondered if telomere-telomere DNA threads present in normal divisions could be stabilized into protein-coated "tethers" when a chromosome is broken. Support for this idea comes from 1) the high frequency of protein-coated tether formation between acentric fragments and segregated chromosomes [23], and 2) the surprisingly high frequency (~40%) that the telomere end of the broken acentric is positioned toward the segregated chromosomes [54]. These studies, and our observation of telomere threads, suggest protein-coated tethers may link to the telomere end of broken acentrics if that end is closest to the segregated chromosomes.

To test if telomere-telomere DNA threads are stabilized into protein-coated tethers upon chromosome breakage, we live imaged dividing neuroblasts co-expressing I-CreI, H2Av-RFP, and the telomere protein HOAP-GFP. As histones are one of the proteins recruited to tethers [23], expression of H2Av-RFP allowed visualization of both chromosomes and tethers. We found histones were recruited to tethers extending from the broken ends of acentrics (Figure 4A, magenta arrow; Video S1) and also from the HOAP-GFP-marked telomere ends of acentrics (Figure 4B, magenta arrowhead; Video S2). We observed histone-coated tethers between the telomeres of acentric fragments and daughter nuclei that connected non-sister telomeres, as the sister acentric fragments were either segregating to the opposing nucleus or co-segregating with the tethered acentric and thus not in the daughter nucleus (Figure 4B). Acentric fragments connected by their telomeres to segregated chromosomes could still move poleward. Additionally, we sometimes observed histone-coated tethers extending off both broken and telomere ends of acentrics simultaneously (Figure 4C), sometimes connecting sister acentrics. We observed H2Av-RFP tethers from the broken ends of 51/90 acentrics (57%), from the telomere ends of 28/90 acentrics (31%), and from both ends of 15/90 acentrics (17%) (Figure 4D). 36/90 (40%) and 13/90 (14%) of acentrics had detectable H2Av-RFP tethers off only their broken or telomere end, respectively (Figure 4D). These results indicate sister and non-sister telomere DNA threads can recruit histones following chromosome breakage.

Telomere DNA threads recruit tether proteins upon chromosome breakage

Histone-coated telomere threads connecting broken acentrics may serve as a platform upon which "tether" proteins localize. Tethers connecting the broken ends of acentric and centric fragments recruit a set of proteins: BubR1, Bub3, Fizzy, Polo, Aurora B, INCENP, and BAF [23,43,44]. These proteins aid in the segregation and incorporation of acentric fragments into daughter nuclei [23,41–44]. As acentric fragments segregated to the nuclei to which they were connected by their telomeres (Figure 4B), we wondered if the tether proteins--specifically BubR1, Polo, Aurora B, and BAF--localized to the telomere threads of broken acentrics. We used single acentrics forming tethers from both their broken and telomere ends (Figure 4C) as the readout for tether protein recruitment to telomere threads. As I-CreI expression generates 4 distinct acentric fragments, we first identified the 4 acentrics, then tracked individual acentrics to assay tether formation from both ends (Figure 5A, labeled 1–4 Figure 5B-E).

To determine if tether proteins are recruited to threads extending from the telomeres of broken acentrics, we live imaged dividing neuroblasts co-expressing I-CreI, H2Av-RFP, and BubR1-EGFP. Consistent with previous reports [23], BubR1-EGFP formed tethers connecting broken acentrics to daughter nuclei (Figure 5B, arrows; Video S3). However, we also observed BubR1-EGFP form tethers between acentrics segregating to opposing poles (Figure 5B, arrowhead). Importantly, we observed instances of single acentrics with BubR1-EGFP tethers extending from both their ends (Figure 5B, zoom). We observed similar results with GFP-Polo (Figure 5C; Video S4), GFP-Aurora B (Figure 5D; Video S5), and GFP-BAF (Figure 5E; Video S6). Therefore, telomere DNA threads recruit BubR1, Polo, Aurora B, and BAF upon chromosome breakage.

To determine if the recruitment of tether proteins to telomere threads only occurs following chromosome breakage, we live imaged neuroblasts with unbroken chromosomes co-expressing H2Av-RFP and BubR1-EGFP. We were unable to detect either BubR1-EGFP or H2Av-RFP localization between segregating chromosomes (Figure 5F), consistent with previous reports [23]. Even in instances when chromosomes were slightly lagging with their ends directly opposed to one another, conditions in which we readily observed DNA threads by DAPI staining, we were unable to detect BubR1-EGFP tethers or BubR1-EGFP on telomeres (Figure 5F'; Video S7). Collectively, we detected BubR1-EGFP tethers in 16/16 cells dividing with broken acentrics, and 42/58 (72%) of acentrics in those cells contained at least one BubR1-EGFP tether (Figure 5G). Of those 42 acentrics with at least one BubR1-EGFP tether, we detected BubR1-EGFP emanating from the other end for 9 acentrics (21%). 0/24 divisions with unbroken chromosomes contained BubR1-EGFP tethers (Figure 5G). These results suggest tether proteins are recruited to telomere threads upon chromosome breakage.

Tether proteins are recruited before anaphase

We next analyzed the timing with which tether proteins localized to the telomere threads of broken acentrics. As previously reported [23,45], BubR1 (Figure S3C, green arrowheads), Polo, and Aurora B all associated with acentrics (Figure S3C, magenta arrows) before anaphase (Figure S3D, grey dots, mean times=144 (BubR1), 116 (Polo), and 186 (Aurora B)

before anaphase onset). These pools became tethers (Figure S3C, green arrows) soon after anaphase entry (Figure S3D, green dots, mean=101 (BubR1), 82 (Polo), and 54 (Aurora B) sec after anaphase onset). In contrast, GFP-BAF localized to acentrics (Figure 3E, asterisks, mean=244 sec after anaphase onset) then tethers (Figure S3E, green arrows, mean=276 sec after anaphase onset) well after anaphase onset (Figure S3D-E). This delay in BAF localization is because VRK1 phosphorylation disrupts the interaction between BAF and DNA in early mitosis [55,56]. While we could not discern if the observed BubR1, Polo, and Aurora B tethers originated from the broken or telomere ends of acentrics, we regularly observed BAF simultaneously localize to tethers off both ends of single acentrics (Figure S3E, green arrows and arrowheads). Additionally, we did not observe multiple patterns in the timing with which BubR1, Aurora B, and Polo formed visible tethers (Figure S3D) despite acentrics segregating with their telomere end first ~40% of the time [54]. Instead, tethers consistently became visible in the first timepoint when acentrics were spatially distinct from segregating chromosome arms. These results suggest tether proteins localize to the broken and telomere ends of acentrics with similar dynamics. Therefore, the recruitment of tether proteins to telomere threads likely occurs before anaphase.

Broken chromosomes result in persistence and stabilization of telomere DNA threads

To quantify how chromosome breakage affects resolution of telomere threads, we compared the timing of thread resolution for 700 seconds after anaphase onset between divisions with and without acentrics. Because BAF, which is enriched on acentrics and tethers [43], also localizes generally to DNA in late anaphase [57], we analyzed GFP-BAF localization to telomere DNA threads in divisions with unbroken chromosomes. No detection of BAF on threads in normal divisions would suggest threads had been resolved before BAF localizes to DNA at the end of mitosis. Consistent with thread resolution occurring in mid-to-late anaphase, we never observed GFP-BAF threads connecting BAF-coated daughter nuclei in divisions with unbroken chromosomes (Figure S3F-G). In contrast, in divisions with broken acentrics, we observed GFP-BAF tethers emanating from both ends of single acentrics that persisted for up to 700 sec after anaphase onset (Figure S3G). Thus, chromosome breakage dramatically increases the persistence of telomere threads.

Broken end tether integrity requires BubR1 activity [23,44]. To determine if global BubR1 activity affects the telomere threads of broken acentrics, we monitored threads in neuroblasts co-expressing I-CreI and a truncated, dominant negative version of BubR1 (UAS-BubR1-DN). In UAS-BubR1-DN neuroblasts, threads connected acentrics in 16/19 of divisions imaged (Figure S3H). 5/19 divisions had threads emanating from both ends of individual acentrics (Figure S3H, arrow and arrowhead), suggesting telomere threads may not require global BubR1 activity to form. However, BubR1 interacts with Bub3 to localize to the broken end tether [44]. The truncated version of BubR1 lacks its full Bub3 binding domain and so may not robustly affect tether integrity. Therefore, future research should determine how BubR1 and other broken end tether proteins contribute to the persistence of telomere threads after chromosome breakage. Nevertheless, these results, and our observations of threads originating from the telomeres of undamaged chromosomes lacking detectable BubR1 (Figures 1, 5), are consistent with a model in which telomere threads on acentrics precede protein-coated tethers and do not rely on the activity of tether proteins for their

initial formation. Collectively, these results suggest normally resolved telomere threads may be stabilized into functional tethers upon chromosome breakage.

Telomere DNA threads from nearby chromosomes may also be stabilized upon chromosome breakage

Recruitment of tether proteins to telomere DNA threads upon chromosome breakage indicates tether formation is not limited to broken ends. However, in divisions with broken chromosomes, we did not observe any tether proteins localize to the DNA threads emanating from the telomeres of segregating unbroken chromosomes (Figure 5B-E). This suggests thread-to-tether stabilization does not occur globally following chromosome breakage but instead is limited to nearby chromosome ends. Recognition of a double-stranded DNA break promotes broken end tether formation [45]. Therefore, recruitment of tether proteins to the DNA threads on the telomeres of broken acentric fragments represents *cis*-stabilization.

To evaluate *trans*-stabilization of threads from the telomeres of nearby unbroken chromosomes, we expressed I-CreI in cells bearing the extra-long In(3LR) chromosome. Unlike the ends of normal-length chromosomes, the ends of extra-long In(3LR) chromatids are close to the broken ends of acentric fragments (Figure S4A). Should *trans*-stabilization occur, normally-resolved threads between the telomeres of the extra-long chromatids may persist, potentially causing bridging, aneuploidy, cell cycle arrest, or death (Figure S4A). We found larvae expressing I-CreI or bearing the In(3LR) extra-long chromosome alone both developed into flies with normal tissues. In contrast, In(3LR) larvae expressing I-CreI developed into flies with nicked wings (Figure S4B, arrows) at a small, significantly increased frequency (I-CreI=3%, N=136; In(3LR)=0%, N=46; I-CreI+In(3LR)=11%, N=176; two-sided Fisher's exact test p=0.003). Wing nicks result from defective proliferation during development [58]. Therefore, I-CreI+In(3LR) cells may arrest or die, potentially from aneuploidy after stabilization of telomere-telomere threads between the extra-long chromatids (Figure S4C). These results suggest *trans*-stabilization of telomere threads may occur rarely. Additionally, the low rate of wing defects in adults developed from larvae with either extra-long chromosomes (threads resolved) or broken acentrics (threads stabilized) illustrates how selective stabilization of telomere threads efficiently maintains genomic integrity.

Discussion

Successful mitosis requires accurate segregation of sister chromatids. Improper segregation leads to aneuploidy [32]. Traditionally, the metaphase-to-anaphase transition is considered the point at which duplicated sister chromatids separate. However, our observation that separating chromosomes remain connected by telomere-telomere DNA threads in most early anaphase *Drosophila* neuroblasts (Figure 1) supports a model that genome separation is largely incomplete until late anaphase [25,26]. Anaphase inter-chromosomal connections often originate at centromeres and telomeres and have been observed in diverse species [17,18,21,22,59]. If unresolved, these connections threaten the genomic integrity of dividing cells [15,26,31–33]. The functional significance of anaphase inter-chromosomal connections is poorly understood.

Here, we propose a model in which pervasive DNA threads between sister and non-sister telomeres can be co-opted to retain lagging chromosomes that would otherwise result in aneuploidy (Figure 6A). Our results indicate inter-chromosomal DNA threads are resolved in mid-to-late anaphase of normal divisions (Figure 6B) but are stabilized into protein-coated tethers if they are near a double-stranded DNA break--such as on a lagging broken fragment. Stabilized tethers may then mediate efficient rescue of the lagging chromosome (Figure 6C). The retention of a potentially lost chromosome may partially balance the threat of aneuploidy these anaphase inter-chromosomal connections pose.

Formation and resolution of inter-chromosomal DNA threads

We observed DNA threads emanating from or near the capped telomeres of anaphase chromosomes (Figure 1). While this suggests telomeres may be conducive to threads, further research is required to determine if threads are composed of telomere, telomere associated, and/or other DNA sequences. Threads may be due to the unique nature of *Drosophila* telomeres. *Drosophila* lack telomerase and maintain their telomeres through retrotransposon activity and homologous recombination [60]. *Drosophila* telomeres can associate with one another, sometimes forming “ectopic fibers” in polytene chromosome preparations [61–63]. Additionally, strong associations between chromosome ends in *Drosophila* strains with long telomeres persist into anaphase before resolving [59]. However, while long telomere associations form pronounced chromosome bridges in anaphase [59], we do not observe any chromosome bridging in our fixed divisions. Instead, linked telomeres are separated by large distances (Figure 2). Furthermore, the DNA telomere-telomere threads we observe lack detectable histones (Figures S1, 5), suggesting threads may be highly stretched. Consistent with this view, threads between extra-long chromosomes, which are presumably under less tension, can occasionally recruit histones (Figure S1). Thus, telomeric DNA threads may be more similar to ultrafine bridges than to traditional chromosome bridges.

Ultrafine bridges commonly originate from centromeres but can also form at telomeres [26,64,65]. Telomere-based ultrafine bridges may contribute to telomere maintenance through “telomere sharing” between telomere-free and telomere-containing chromosome ends [27], which might be more common in telomerase-lacking *Drosophila*. One cause of ultrafine bridges is replication-induced catenation between sister chromatids [17,18,66]. Our observation of DNA threads between the telomeres of extra-long sister chromatids (Figure 2) is consistent with threads resulting from replication-induced catenation. However, creation of unbroken acentrics by FLP-mediated recombination places both sister telomeres on the same unbroken acentric (Figure 3). Therefore, threads connecting the intact, non-sister telomeres of unbroken acentrics and the telomeres of segregated chromosomes (Figure 3) suggests other mechanisms besides catenation contribute to the formation of these threads. Other potential mechanisms include homologous recombination or late replication intermediates [29,67].

Regardless of how threads form, normally dividing cells must resolve the threads to preserve euploidy. We believe that before resolution, threads become so stretched they become undetectable. It is likely highly stretched, but invisible, threads are included in our (−) classification. We expect stretched threads would be susceptible to nucleases, such as

Ankle1 [68], or factors that resolve bridges, such as BLM helicase [18]. Thus, recently resolved threads likely contribute to the (−) classification as well. Since we cannot differentiate between highly stretched, invisible threads and recently resolved threads, we consider the (−) classification to span the period of resolution. Thread resolution occurs in mid-to-late anaphase (Figure 1) primarily through a spatial mechanism (Figure 2). The spatial resolution mechanism likely accounts for the persistence of DNA threads connecting segregated chromosomes to closely associated lagging chromosomes (Figure 3).

Stabilization of telomere DNA threads into protein-coated tethers

Upon chromosome breakage, sister and non-sister telomere DNA threads recruit a set of tether proteins: histones, BubR1, Polo, Aurora B, and BAF (Figures 4–5). Previous research has demonstrated these proteins play important roles in the segregation and incorporation of broken chromosomes into daughter nuclei [23,41,42,44]. Considering 1) telomere threads can ostensibly transmit force between unbroken chromosome ends (Figure S2) and 2) threads on broken acentrics persist through late anaphase well after they would have normally been resolved (Figures 3 and S3), chromosome breakage may preserve threads and provide a platform for the recruitment of tether proteins that subsequently retain the broken chromosome fragment. Indeed, acentrics often segregate toward and reintegrate into daughter nuclei with their telomere ends leading [54]. It seems plausible the integration of these telomere-leading acentrics could be mediated by telomere tethers. Thus, telomere DNA threads that have been stabilized into tethers could aid in persevering genome integrity.

We do not know how tether proteins are recruited to telomere DNA threads upon chromosome breakage. One possibility is the telomere end is recognized as a DNA break. Recognizing a double-stranded DNA break is key for the recruitment of proteins to the broken end of chromosome fragments [45]. However, HOAP-GFP localization on the natural ends of broken acentrics suggests the acentric telomeres are intact and capped (Figure 4) and should not be recognized as broken ends [69]. An alternate possibility is the initial recruitment of proteins to the broken ends results in “leaky” recruitment of proteins to the telomere DNA threads, either by 1) direct recruitment to any chromosome thread near a recognized broken end or 2) recruitment first to the broken end then relocation to the telomere thread.

Like their recruitment to the broken end [23,45], tether protein recruitment to telomere end threads probably initiates before anaphase (Figure S3). Additionally, tether proteins localize to damage induced specifically during anaphase [45], indicating recruitment continues throughout anaphase. Accordingly, BAF localizes to both the broken end and telomere tethers simultaneously during late anaphase (Figure S3). Sustained recruitment of tether proteins to the telomere end before and during anaphase could contribute to the increased persistence of telomere threads following chromosome breakage.

General telomere inter-chromosomal DNA threads may lead to efficient recovery of broken chromosome fragments

Retention of genetic material that would otherwise be lost in division is not a unique feature of *Drosophila* (for review, see [37]). Retention can occur through multiple mechanisms. For example, proteinaceous filaments retain chromosome fragments in human cells [47].

Additionally, double minute chromosomes are transported by attaching to the arms of segregating centric chromosomes [70,71]. Furthermore, lateral microtubule connections also mediate segregation of acentric chromosomes in insects and trypanosomes [54,72,73]. Efficiency of these mechanisms vary. Overall, many chromosome fragments are not retained and instead form damage-prone micronuclei [8]. However, chromosome fragment retention in *Drosophila* occurs with remarkable fidelity [23,35].

Selective stabilization of prevalent telomere DNA threads into protein-coated tethers offers a potential explanation for the high efficacy of broken chromosome retention in *Drosophila*. In addition to lateral connections with microtubules [54], tether proteins are important for both the timely poleward segregation of acentrics [23] and their integration into daughter nuclei [41–43]. Thus, the ability to form tethers off either the broken or telomere end of an acentric may enhance the ability to retain that fragment (Figure 6C). Additionally, a pre-formed network of telomeric DNA threads may allow for a more rapid response to retaining broken chromosomes. However, until the function of telomere threads can be experimentally tested in both normal divisions and in divisions with broken chromosomes, it is possible telomere threads are only involved passively in chromosome segregation. Future research is therefore required to test these ideas. Collectively, our results suggest a novel mechanism in which pervasive anaphase inter-chromosomal connections could be co-opted to retain wayward chromosomes that would otherwise threaten aneuploidy.

STAR Methods

RESOURCE AVAILABILITY

Lead contact—Further information and requests for resources and reagents should be directed to and will be fulfilled by the lead contact, Brandt Warecki (bwarecki@ucsc.edu).

Materials availability—This study did not generate new unique reagents

Data and code availability

- All data reported in this paper will be shared by the lead contact upon request.
- This paper does not report original code.
- Any additional information required to reanalyze the data reported in this paper is available from the lead contact upon request.

EXPERIMENTAL MODEL AND SUBJECT DETAILS

Drosophila *stocks*—All *Drosophila* stocks were raised on standard brown food [74] at 25°C with a 12h light/dark cycle. The following stocks from the Bloomington Drosophila Stock Center (BDSC) were used in this study: *y1v1* (RRID:BDSC_1509), In(3LR) (RRID:BDSC_1222), C(2)EN (RRID:BDSC_1020), hs-I-CreI (RRID:BDSC_6936), UAS-BubR1-EGFP (RRID:BDSC_91697), UAS-RpA-70-RNAi (RRID:BDSC_35426), UAS-BubR1-DN (RRID:BDSC_8382; generated by Exelixis, Inc.). elav-Gal4 [75] was used to drive expression of UAS-BubR1-EGFP, UAS-GFP-Aurora B, UAS-RpA-70-RNAi, and UAS-BubR1-DN. GFP-Polo and GFP-Aurora B stocks were provided by Dr. Joseph Lipsick

(Stanford University, Stanford, CA) [76]. The GFP-BAF stock was provided by Dr. Pamela Geyer (University of Iowa, Iowa City, IA) [77]. hs-I-CreI (III), hs-FLP, and inverted FRT stocks were provided by Dr. Kent Golic (University of Utah, Salt Lake City, UT) [53,78]. HOAP-GFP stocks were provided by Dr. John Tamkun (University of California, Santa Cruz, Santa Cruz, CA). Timing data for acentric localization and tether formation (Figure S3) was supplemented with additional experiments using GFP-BubR1 [79] and GFP-Polo (RRID:BDSC_84275) stocks.

The genotypes of larvae used for fixing and staining experiments were: *y1v1*=male and female *y1,v1*/*y1,v1* or *y1,v1*/Y (Figures 1, 2, S1); HOAP-GFP=male and female *w**/*w**;;HOAP-GFP/HOAP-GFP or *w**/Y;;HOAP-GFP/HOAP-GFP (Figure 1); elav-Gal4 + UAS-RpA-70-RNAi=female elav-Gal4/*y1,sc*,v1,sev21*;UAS-RpA-70-RNAi/H2Av-RFP (Figure S1); female *y1v1* =+/*y1,v1* (Figure S1); female UAS-RpA-70-RNAi=+/*y1,sc*,v1,sev21*;UAS-RpA-70-RNAi/+ (Figure S1); In(3LR)=male and female In(3LR)264,*mv1*/Tm6B,Tb (Figures 2 and S3); C(2)EN=male and female C(2)EN,*bw1,sp1* (Figures 2 and S3); hs-FLP + inverted FRTs=male and female 105(inverted FRTs)/*w1118*;hs-FLP/+ or 105/Y;hs-FLP/+ (Figure 3); I-CreI=male and female hs-I-CreI.2A,*v1*/hs-I-CreI.2A,*v1*;;*ry506/ry506* or hs-I-CreI.2A,*v1*/Y;;*ry506/ry506* (Figures 3 and S3); I-CreI + elav-Gal4 + UAS-BubR1-DN=female elav-Gal4/*y1,w1118*;H2Av-RFP/+;UAS-BubR1-DN/I-CreI,Sb (Figure S3); and I-CreI + In(3LR)=female hs-I-CreI.2A,*v1*/+;;In(3LR)264,*mv1*/*ry506* (Figure S4).

The genotypes of larvae used for live imaging experiments were: *y1v1*=male *y1,v1*/Y;H2Av-RFP/+ (Figure S1); elav-Gal4 + UAS-RpA-70-RNAi=female elav-Gal4/*y1,sc*,v1,sev21*;UAS-RpA-70-RNAi/H2Av-RFP (Figure S1); H2Av-RFP + In(3LR)=female elav-Gal4/+;H2Av-RFP/+;In(3LR)264,*mv1*/+ (Figure S2); I-CreI + HOAP-GFP=female elav-Gal4/*w**;H2Av-RFP/+;I-CreI,Sb/HOAP-GFP (Figure 4); I-CreI + BubR1-EGFP=female elav-Gal4/*w**;H2Av-RFP/+;hs-I-CreI,Sb/UAS-BubR1-EGFP (Figure 5); I-CreI + GFP-Polo=female elav-Gal4/*+*;H2Av-RFP/+;hs-I-CreI,Sb/Ubi-GFP-Polo (Figure 5); I-CreI + GFP-Aurora B=female elav-Gal4/+;H2Av-RFP/UAS-GFP-Aurora B;hs-I-CreI,Sb/+ (Figure 5); I-CreI + GFP-BAF=female elav-Gal4/*y1,w**;H2Av-RFP/GFP-BAF;hs-I-CreI,Sb/+ (Figure 5 and S3); BubR1-EGFP=female elav-Gal4/*w**;H2Av-RFP/+;UAS-BubR1-EGFP/+ (Figure 5 and S3); and GFP-BAF=female elav-Gal4/*y1,w**;H2Av-RFP/GFP-BAF (Figure S3). Additionally, female elav-Gal4/*w1118*;GFP-BubR1/H2Av-RFP;hs-I-CreI,Sb/+ and female elav-Gal4/*w**;hs-GFP-Polo/H2Av-RFP;hs-I-CreI,Sb/GFP-Polo larvae were used to supplement timing experiments in Figure S3.

The genotypes of larvae/flies used for the wing defect analysis (Figure S4) were: I-CreI=hs-I-CreI.2A,*v1*/*y1,v1*;;*ry506*/+ and hs-I-CreI.2A,*v1*/Y;;*ry506*/+; In(3LR)=*y1,v1*/Y;;In(3LR),*mv1*/+ and *y1v1*/+;;In(3LR),*mv1*/+; I-CreI + In(3LR)=hs-I-CreI.2A,*v1*/Y;;In(3LR),*mv1*/*ry506* and hs-I-CreI.2A,*v1*/+;;In(3LR),*mv1*/*ry506*. For experiments involving both male and female larvae/adults, analysis of the influence of sex was not performed as sex was not expected to be pertinent for these experiments.

Cancer cell culture—PC-3 prostate adenocarcinoma cells that had been derived from a 62 year-old male (RRID:CVCL_0035) were grown at 37°C in a 95%-air/5%-CO_2

atmosphere. Cells were grown in F-12K medium (Gibco) supplemented with 10% fetal bovine serum (Gibco). Cells were maintained in logarithmic growth phase by splitting with a Trypsin-EDTA mixture. Cell authentication was not performed prior to experiments.

METHOD DETAILS

Generation of broken and unbroken acentrics—Broken acentrics were generated by expressing hs-I-CreI through a 1 h 37°C heatshock of 3rd instar larvae. Larvae were allowed to recover for 1 h before dissection. Larvae were dissected for a period of 1–4 h after heatshock. The I-CreI endonuclease recognizes its cut site in the base of the *Drosophila* X and Y chromosomes [53]. Therefore, I-CreI expression in female larvae resulted in 4 acentrics. Unbroken acentrics were generated by expressing hs-FLP through 1 h 37°C heatshock of 3rd instar larvae containing the 105 inverted FRTs transgene [14]. Larvae were allowed to recover for 1 h before dissection. Larvae were dissected for a period of 1–4 h after heatshock.

Fixed neuroblast cytology—Larval brains were dissected in 0.7% NaCl and fixed in 3.7% formaldehyde for 30 min. Dissected brains were washed in 45% acetic acid in PBS, squashed between siliconized coverslips and glass slides in 60% acetic acid in PBS, then frozen in liquid nitrogen for at least 10 min. Slides were washed in 20% ethanol (10 min at −20°C), PBS + Triton X-100 (PBST; 10 min) and PBS (2 × 5 min). Slides were blocked for 1h in 5% dried milk in PBST. Slides were washed in PBST (3 × 5 min) then stained with DAPI in Vectashield (Vector Laboratories Cat# H-1200, RRID:AB_2336790). For neuroblasts stained with PI, samples were prepared as above with an overnight RNA digestion step (RNAse A 2.5 mg/mL in PBST) prior to blocking. After the final 3 PBST washes, samples were stained with PI (20 ug/mL in 70% glycerol/30% PBS).

Immunofluorescence—Larval brains were dissected in 0.7% NaCl and fixed in 3.2% paraformaldehyde. Brains were immediately squashed between siliconized coverslips and glass slides in 3.2% paraformaldehyde then frozen in liquid nitrogen for at least 10 min. Slides were incubated with chicken anti-GFP antibody (Aves Labs Cat# GFP-1010, RRID:AB_2307313) at 1:500 in 1X PBS 1% BSA + 0.05% Triton X-100 (PBT) for 1h at room temperature. Slides were rinsed in PBT then stained with anti-chicken-Alexa488 (Thermo Fisher Scientific Cat# A-11039, RRID:AB_2534096) at 1:500 in PBT for 1h at room temperature. Slides were rinsed in PBT, then counterstained with DAPI in Vectashield.

Live neuroblast cytology—Larval brains were dissected in PBS and placed in 17 μL of PBS between a slide and a coverslip. PBS was wicked away to induce gentle squashing [79]. Coverslips were outlined with halocarbon oil, and slides were imaged immediately. We filmed neuroblasts along the periphery of the brain. Slides were imaged for up to 1 h maximum before a new dissection [80]. Imaging was performed using a spinning disk confocal (Figure 4–5, S1, S2, S3) or a wide-field (Figure S1) microscope.

Cancer cell cytology—Prior to fixing, PC-3 cells were first split into 2-well chamber slides (ThermoFisher Scientific) and allowed to adhere for 2 days (media changed after first night). For fixing, slides were placed on ice for 30 min, after which cells were fixed in 4% paraformaldehyde in PHEM buffer for 20 min. Slides were rinsed with PBST for 2 min

and blocked with 5% BSA in PHEM for 1 h. Cells were stained with rabbit-anti-LaminB1 (1:1000 in PBS; Abcam Cat# ab16048, RRID:AB_443298) overnight at 4°C. The following day, slides were washed twice with PBS (5 min each), stained with anti-rabbit-Alexa488 (1:1000; Thermo Fisher Scientific Cat# A-11008, RRID:AB_143165) and washed twice more with PBS (5 min each). Slides were counterstained with DAPI in Vectashield.

Microscopy and image acquisition

Airyscan microscopy: Super-resolution images were acquired with an AxioObserver.Z1 Zeiss 880 confocal microscope equipped with an Airyscan detector and 63× 1.4 NA Plan-Apochromat objective. Imaging was performed at room temperature. For DAPI, samples were illuminated with a 405 nm laser. For PI, samples were illuminated with a 561 nm laser. For Alexa488, samples were illuminated with a 488 nm laser. Data were collected with 420–480 and 495–550 band pass and 605 long pass filters. Images were collected and processed using the Airyscan mode with Zen Black software (Zeiss) and deconvolved using Zen Blue (Zeiss).

Spinning-disk confocal microscopy: Time-lapse imaging was performed on an inverted Eclipse TE2000-E spinning disk (CSL1-X1; Nikon) confocal microscope equipped with a Hamamatsu electron-multiplying charge couple device camera (ImageEM X2) and a 100× 1.4 NA oil immersion objective. 488 and 561 nm lasers were used to excited GFP and RFP respectively. Imaging was performed at room temperature. Successive timepoints were filmed at 10–18 s. Images were acquired with MicroManager 1.4 software.

Wide-field microscopy: Time-lapse imaging was performed with a Leica DM16000B wide-field inverted microscope with a Hamamatsu electron-multiplying charge coupled device camera (ORCA 9100–02) with a binning of 1 and a 100× 1.4 NA Plan-Apochromat objective. Successive timepoints were filmed at 20 s. Imaging was performed at room temperature. Images were acquired with Leica Application Suite Advanced Fluorescence software and 3D deconvolved using AutoQuant X2.2.0 software.

Scanning confocal microscopy: Fixed and stained PC-3 cells were imaged on an inverted Leica DMI6000 SP5 scanning confocal microscope. DAPI was excited with a 405 nm laser, and emission was collected from 410–470 nm. Alexa488 was excited with a 488 nm laser, and emission was collected from 503–538 nm. Imaging was performed at room temperature. Images were acquired with Leica Application Suite Advanced Fluorescence (Leica) software.

Image processing—The brightness and contrast of images acquired from Airyscan super-resolution experiments were adjusted to score for the presence or absence of inter-chromosomal threads. Often, this meant saturating the signal from the main chromosome masses. Original, unsaturated images of the main chromosome masses are shown with each adjusted image.

Figure preparation—Imaging data was processed in Fiji, and figures were assembled in Adobe Illustrator. Maximum projections are shown for all images unless otherwise

indicated. To improve clarity when appropriate, individual images were adjusted for brightness and contrast. Graphs were created using the ggplot2 package [81] in R.

Experimental design—Specific sample sizes were not estimated prior to experimentation. Instead, each experiment was performed at least 3 independent times. Experiments were performed and analyzed unblinded. For comparisons between different conditions, experiments were performed during the same time period. We did not score 1) anaphase divisions in which the ends of chromosomes were not visually separated or 2) anaphase divisions in which another cell was fixed in plane between separating chromosome masses, as it was impossible to accurately assay for the presence and strength of threads in these situations. All other anaphase divisions were included in analyses.

QUANTIFICATION AND STATISTICAL ANALYSIS

Quantification—Threads were classified and scored as described in Figure 1A-D. We scored divisions as containing threads if we were able to observe ++ (complete, uninterrupted DAPI staining connecting chromosome tips) or + (complete DAPI staining connecting chromosome tips with small gaps in the DAPI staining). We scored divisions as lacking threads if we observed - (DAPI staining from only one chromosome tip) or -- (no apparent DAPI staining) threads. To minimize any confounding background noise, we scored for the presence or absence of threads by analyzing single brightness/contrast enhanced z-slices from an acquired z-stack. Anaphase stage was scored as follows: early=chromosome ends separated by < half the length of a chromosome arm, mid=chromosome ends separated by between half to twice the length of a chromosome arm, or late=chromosome ends separated by greater than twice the full length of a chromosome arm or chromosome arms are decondensed. Representative early, mid, and late anaphases are shown in Figure 1E.

Distances of thread origins to capped telomeres (Figure 1E) were calculated in x-, y-, and z-three-dimensional space in acquired z-stacks by measuring between the points on chromosome ends from where threads emerged to the edge of the nearest HOAP-GFP signal. Thread distances (Figure 2E-E') were measured by calculating the distance between the ends of connected chromosome tips three-dimensional space in acquired z-stacks. Chromosome lengths (Figure S2A) were measured by calculating the distance in three-dimensional space between the furthest segregated point of a nucleus and the most extended tip of either an extra-long chromosome or a normal-length chromosome.

Histone recruitment to threads (Figure S2C'-E') was measured using the plot profile feature in Fiji. Angle measurements for coordinated chromosome movement (Figure S2G-G') were calculated using the angle tool in Fiji. Normalized thread intensity (Figure 3G) was determined in Fiji by measuring the mean grey value of the thread divided by the mean grey value of a region of interest outside the cell. Timing of tether protein recruitment to acentrics (Figure S3D) was determined as the first timepoint at which tether proteins were visible on chromatin clearly identifiable as acentrics. Timing of tether visibility (Figure S3D) was determined as the first timepoint at which tether proteins formed a linear tether between

spatially distinct chromosomes. For the timings of BubR1 and Polo recruitment, additional data was gathered with secondary stocks containing GFP-BubR1 and GFP-Polo transgenes.

Analyses of the following experiments contributed to data in multiple figures: fixed and DAPI-stained *y1v1* neuroblasts (Figures 1-2, S1), fixed and DAPI-stained In(3LR) neuroblasts (Figures 2 and S2), fixed and DAPI-stained C(2)EN neuroblasts (Figures 2 and S2), and live neuroblasts expressing H2Av-RFP, I-CreI, and BubR1-EGFP (Figures 5 and S3), GFP-Polo (Figures 5 and S3), GFP-Aurora B (Figures 5 and S3), or GFP-BAF (Figures 5 and S3).

Statistical analyses—All statistical analyses were performed in R (R Core Team). Two-sided Fisher's exact tests (Figure 1E', Figure 2D, Figure 3F, Figure S1E, Figure S4B) were performed using 2 × 2 and 3 × 2 contingency tables, when appropriate. Mann-Whitney tests (Figure 2E', Figure 3G, Figure S1F, Figure S2B) and Kruskal-Wallis tests (Figure 2E) were used when comparing two or more continuous datasets respectively. N values refer to the number of neuroblasts analyzed except for: Figure 1G-H' (N=number of thread origins); Figure 3G (N=number of threads); Figure 4D + 5G (N=number of acentrics); and Figure S4B (N=number of flies). N values are listed in either the figure panels, figure legends, and/or written results sections. To show variation, all data were graphed as individual points in dot plots for non-binary continuous datasets. Statistical significance was defined as $p<0.05$ (*), $p<0.01$ (**), $p<0.001$ (***).

Supplementary Material

Refer to Web version on PubMed Central for supplementary material.

Acknowledgements

We thank Dr. Susan Strome and Dr. William Saxton for use of their equipment and for providing reagents. We thank Dr. Benjamin Abrams (UCSC Life Sciences Microscopy Center, RRID: SCR_021135) for his technical support and assistance with microscopy experiments. We thank Dr. Joseph Lipsick, Dr. Pamela Geyer, Dr. Kent Golic, and Dr. John Tamkun for providing fly stocks. We thank Dr. Zhu Wang for providing the PC-3 human cancer cell line. We thank Dr. Camilla Forsberg for providing reagents. Funding for these studies was provided by an NIH grant NIGMS-1R35GM139595 awarded to W. Sullivan. Purchase of the Zeiss 880 confocal microscope used in this research was made possible through the National Institutes of Health s10 Grant 1S10OD23528–01.

REFERENCES

1. McClintock B (1941). The Stability of Broken Ends of Chromosomes in Zea Mays. Genetics 26, 234–282. 10.1093/genetics/26.2.234. [PubMed: 17247004]
2. Gisselsson D, Pettersson L, Hoglund M, Heidenblad M, Gorunova L, Wiegant J, Mertens F, Dal Cin P, Mitelman F, and Mandahl N (2000). Chromosomal breakage-fusion-bridge events cause genetic intratumor heterogeneity. Proc Natl Acad Sci U S A 97, 5357–5362. 10.1073/pnas.090013497. [PubMed: 10805796]
3. Thomas R, Marks DH, Chin Y, and Benezra R (2018). Whole chromosome loss and associated breakage-fusion-bridge cycles transform mouse tetraploid cells. EMBO J 37, 201–218. 10.15252/embj.201797630. [PubMed: 29196303]
4. Ben-David U, and Amon A (2020). Context is everything: aneuploidy in cancer. Nat Rev Genet 21, 44–62. 10.1038/s41576-019-0171-x. [PubMed: 31548659]
5. Maciejowski J, Chatzipli A, Dananberg A, Chu K, Toufektchan E, Klimczak LJ, Gordenin DA, Campbell PJ, and de Lange T (2020). APOBEC3-dependent kataegis and TREX1-driven

chromothripsis during telomere crisis. Nat Genet 52, 884–890. 10.1038/s41588-020-0667-5. [PubMed: 32719516]

6. Maciejowski J, Li Y, Bosco N, Campbell PJ, and de Lange T (2015). Chromothripsis and Kataegis Induced by Telomere Crisis. Cell 163, 1641–1654. 10.1016/j.cell.2015.11.054. [PubMed: 26687355]
7. Crasta K, Ganem NJ, Dagher R, Lantermann AB, Ivanova EV, Pan Y, Nezi L, Protopopov A, Chowdhury D, and Pellman D (2012). DNA breaks and chromosome pulverization from errors in mitosis. Nature 482, 53–58. 10.1038/nature10802. [PubMed: 22258507]
8. Fenech M, Kirsch-Volders M, Natarajan AT, Surralles J, Crott JW, Parry J, Norppa H, Eastmond DA, Tucker JD, and Thomas P (2011). Molecular mechanisms of micronucleus, nucleoplasmic bridge and nuclear bud formation in mammalian and human cells. Mutagenesis 26, 125–132. 10.1093/mutage/geq052. [PubMed: 21164193]
9. Zhang CZ, Spektor A, Cornils H, Francis JM, Jackson EK, Liu S, Meyerson M, and Pellman D (2015). Chromothripsis from DNA damage in micronuclei. Nature 522, 179–184. 10.1038/nature14493. [PubMed: 26017310]
10. Mikhailov A, Cole RW, and Rieder CL (2002). DNA damage during mitosis in human cells delays the metaphase/anaphase transition via the spindle-assembly checkpoint. Curr Biol 12, 1797–1806. 10.1016/s0960-9822(02)01226-5. [PubMed: 12419179]
11. Royou A, Macias H, and Sullivan W (2005). The Drosophila Grp/Chk1 DNA damage checkpoint controls entry into anaphase. Curr Biol 15, 334–339. 10.1016/j.cub.2005.02.026. [PubMed: 15723794]
12. Corbett KD (2017). Molecular Mechanisms of Spindle Assembly Checkpoint Activation and Silencing. Prog Mol Subcell Biol 56, 429–455. 10.1007/978-3-319-58592-5_18. [PubMed: 28840248]
13. van Steensel B, Smogorzewska A, and de Lange T (1998). TRF2 protects human telomeres from end-to-end fusions. Cell 92, 401–413. 10.1016/s0092-8674(00)80932-0. [PubMed: 9476899]
14. Titen SW, and Golic KG (2008). Telomere loss provokes multiple pathways to apoptosis and produces genomic instability in Drosophila melanogaster. Genetics 180, 1821–1832. 10.1534/genetics.108.093625. [PubMed: 18845846]
15. Germann SM, Schramke V, Pedersen RT, Gallina I, Eckert-Boulet N, Oestergaard VH, and Lisby M (2014). TopBP1/Dpb11 binds DNA anaphase bridges to prevent genome instability. J Cell Biol 204, 45–59. 10.1083/jcb.201305157. [PubMed: 24379413]
16. Quevedo O, and Lisby M (2018). Imaging of DNA Ultrafine Bridges in Budding Yeast. Methods Mol Biol 1672, 483–493. 10.1007/978-1-4939-7306-4_32. [PubMed: 29043643]
17. Baumann C, Korner R, Hofmann K, and Nigg EA (2007). PICH, a centromere-associated SNF2 family ATPase, is regulated by Plk1 and required for the spindle checkpoint. Cell 128, 101–114. 10.1016/j.cell.2006.11.041. [PubMed: 17218258]
18. Chan KL, North PS, and Hickson ID (2007). BLM is required for faithful chromosome segregation and its localization defines a class of ultrafine anaphase bridges. EMBO J 26, 3397–3409. 10.1038/sj.emboj.7601777. [PubMed: 17599064]
19. Wang LH, Schwarzbraun T, Speicher MR, and Nigg EA (2008). Persistence of DNA threads in human anaphase cells suggests late completion of sister chromatid decatenation. Chromosoma 117, 123–135. 10.1007/s00412-007-0131-7. [PubMed: 17989990]
20. Naim V, and Rosselli F (2009). The FANC pathway and BLM collaborate during mitosis to prevent micro-nucleation and chromosome abnormalities. Nat Cell Biol 11, 761–768. 10.1038/ncb1883. [PubMed: 19465921]
21. Ono M, Preece D, Duquette ML, Forer A, and Berns MW (2017). Mitotic tethers connect sister chromosomes and transmit “cross-polar” force during anaphase A of mitosis in PtK2 cells. Biomed Opt Express 8, 4310–4315. 10.1364/BOE.8.004310. [PubMed: 29082066]
22. LaFountain JR Jr., Cole RW, and Rieder CL (2002). Partner telomeres during anaphase in crane-fly spermatocytes are connected by an elastic tether that exerts a backward force and resists poleward motion. J Cell Sci 115, 1541–1549. [PubMed: 11896200]

23. Royou A, Gagou ME, Karess R, and Sullivan W (2010). BubR1- and Polo-coated DNA tethers facilitate poleward segregation of acentric chromatids. Cell 140, 235–245. 10.1016/j.cell.2009.12.043. [PubMed: 20141837]
24. Forer A, and Berns MW (2020). Elastic Tethers Between Separating Anaphase Chromosomes Regulate the Poleward Speeds of the Attached Chromosomes in Crane-Fly Spermatocytes. Front Mol Biosci 7, 161. 10.3389/fmolb.2020.00161. [PubMed: 32850955]
25. Paliulis LV, and Forer A (2018). A review of "tethers": elastic connections between separating partner chromosomes in anaphase. Protoplasma 255, 733–740. 10.1007/s00709-017-1201-1. [PubMed: 29307016]
26. Fernandez-Casanas M, and Chan KL (2018). The Unresolved Problem of DNA Bridging. Genes (Basel) 9. 10.3390/genes9120623.
27. Stroik S, and Hendrickson EA (2020). Telomere fusions and translocations: a bridge too far? Curr Opin Genet Dev 60, 85–91. 10.1016/j.gde.2020.02.010. [PubMed: 32171975]
28. Liu Y, Nielsen CF, Yao Q, and Hickson ID (2014). The origins and processing of ultra fine anaphase DNA bridges. Curr Opin Genet Dev 26, 1–5. 10.1016/j.gde.2014.03.003. [PubMed: 24795279]
29. Chan YW, Fugger K, and West SC (2018). Unresolved recombination intermediates lead to ultra-fine anaphase bridges, chromosome breaks and aberrations. Nat Cell Biol 20, 92–103. 10.1038/s41556-017-0011-1. [PubMed: 29255170]
30. Hengeveld RC, de Boer HR, Schoonen PM, de Vries EG, Lens SM, and van Vugt MA (2015). Rif1 Is Required for Resolution of Ultrafine DNA Bridges in Anaphase to Ensure Genomic Stability. Dev Cell 34, 466–474. 10.1016/j.devcel.2015.06.014. [PubMed: 26256213]
31. Baxter J (2015). "Breaking up is hard to do": the formation and resolution of sister chromatid intertwines. J Mol Biol 427, 590–607. 10.1016/j.jmb.2014.08.022. [PubMed: 25194916]
32. Finardi A, Massari LF, and Visintin R (2020). Anaphase Bridges: Not All Natural Fibers Are Healthy. Genes (Basel) 11. 10.3390/genes11080902.
33. Broderick R, Nieminuszczy J, Blackford AN, Winczura A, and Niedzwiedz W (2015). TOPBP1 recruits TOP2A to ultra-fine anaphase bridges to aid in their resolution. Nat Commun 6, 6572. 10.1038/ncomms7572. [PubMed: 25762097]
34. Bollen Y, Stelloo E, van Leenen P, van den Bos M, Ponsioen B, Lu B, van Roosmalen MJ, Bolhaqueiro ACF, Kimberley C, Mossner M, et al. (2021). Reconstructing single-cell karyotype alterations in colorectal cancer identifies punctuated and gradual diversification patterns. Nat Genet 53, 1187–1195. 10.1038/s41588-021-00891-2. [PubMed: 34211178]
35. Bretscher HS, and Fox DT (2016). Proliferation of Double-Strand Break-Resistant Polyploid Cells Requires Drosophila FANCD2. Dev Cell 37, 444–457. 10.1016/j.devcel.2016.05.004. [PubMed: 27270041]
36. Ly P, Teitz LS, Kim DH, Shoshani O, Skaletsky H, Fachinetti D, Page DC, and Cleveland DW (2017). Selective Y centromere inactivation triggers chromosome shattering in micronuclei and repair by non-homologous end joining. Nat Cell Biol 19, 68–75. 10.1038/ncb3450. [PubMed: 27918550]
37. Warecki B, and Sullivan W (2020). Mechanisms driving acentric chromosome transmission. Chromosome Res 28, 229–246. 10.1007/s10577-020-09636-z. [PubMed: 32712740]
38. Orr B, De Sousa F, Gomes AM, Afonso O, Ferreira LT, Figueiredo AC, and Maiato H (2021). An anaphase surveillance mechanism prevents micronuclei formation from frequent chromosome segregation errors. Cell Rep 37, 109783. 10.1016/j.celrep.2021.109783. [PubMed: 34758324]
39. Afonso O, Castellani CM, Cheeseman LP, Ferreira JG, Orr B, Ferreira LT, Chambers JJ, Morais-de-Sa E, Maresca TJ, and Maiato H (2019). Spatiotemporal control of mitotic exit during anaphase by an aurora B-Cdk1 crosstalk. Elife 8. 10.7554/eLife.47646.
40. Afonso O, Matos I, Pereira AJ, Aguiar P, Lampson MA, and Maiato H (2014). Feedback control of chromosome separation by a midzone Aurora B gradient. Science 345, 332–336. 10.1126/science.1251121. [PubMed: 24925910]
41. Karg T, Warecki B, and Sullivan W (2015). Aurora B-mediated localized delays in nuclear envelope formation facilitate inclusion of late-segregating chromosome fragments. Mol Biol Cell 26, 2227–2241. 10.1091/mbc.E15-01-0026. [PubMed: 25877868]

42. Warecki B, and Sullivan W (2018). Micronuclei Formation Is Prevented by Aurora B-Mediated Exclusion of HP1a from Late-Segregating Chromatin in Drosophila. Genetics 210, 171–187. 10.1534/genetics.118.301031. [PubMed: 29986897]
43. Warecki B, Ling X, Bast I, and Sullivan W (2020). ESCRT-III-mediated membrane fusion drives chromosome fragments through nuclear envelope channels. J Cell Biol 219. 10.1083/jcb.201905091.
44. Derive N, Landmann C, Montembault E, Claverie MC, Pierre-Elies P, Goutte-Gattat D, Founounou N, McCusker D, and Royou A (2015). Bub3-BubR1-dependent sequestration of Cdc20Fizzy at DNA breaks facilitates the correct segregation of broken chromosomes. J Cell Biol 211, 517–532. 10.1083/jcb.201504059. [PubMed: 26553926]
45. Landmann C, Pierre-Elies P, Goutte-Gattat D, Montembault E, Claverie MC, and Royou A (2020). The Mre11-Rad50-Nbs1 complex mediates the robust recruitment of Polo to DNA lesions during mitosis in Drosophila. J Cell Sci 133. 10.1242/jcs.244442.
46. Clay DE, Bretscher HS, Jezuit EA, Bush KB, and Fox DT (2021). Persistent DNA damage signaling and DNA polymerase theta promote broken chromosome segregation. J Cell Biol 220. 10.1083/jcb.202106116.
47. Leimbacher PA, Jones SE, Shorrocks AK, de Marco Zompit M, Day M, Blaauwendraad J, Bundschuh D, Bonham S, Fischer R, Fink D, et al. (2019). MDC1 Interacts with TOPBP1 to Maintain Chromosomal Stability during Mitosis. Mol Cell 74, 571–583 e578. 10.1016/j.molcel.2019.02.014. [PubMed: 30898438]
48. Cenci G, Siriaco G, Raffa GD, Kellum R, and Gatti M (2003). The Drosophila HOAP protein is required for telomere capping. Nat Cell Biol 5, 82–84. 10.1038/ncb902. [PubMed: 12510197]
49. Mitsis PG, Kowalczykowski SC, and Lehman IR (1993). A single-stranded DNA binding protein from Drosophila melanogaster: characterization of the heterotrimeric protein and its interaction with single-stranded DNA. Biochemistry 32, 5257–5266. 10.1021/bi00070a038. [PubMed: 8494903]
50. Liu T, and Huang J (2016). Replication protein A and more: single-stranded DNA-binding proteins in eukaryotic cells. Acta Biochim Biophys Sin (Shanghai) 48, 665–670. 10.1093/abbs/gmw041. [PubMed: 27151292]
51. Oliveira RA, Kotadia S, Tavares A, Mirkovic M, Bowlin K, Eichinger CS, Nasmyth K, and Sullivan W (2014). Centromere-independent accumulation of cohesin at ectopic heterochromatin sites induces chromosome stretching during anaphase. PLoS Biol 12, e1001962. 10.1371/journal.pbio.1001962. [PubMed: 25290697]
52. Novitski E, Grace D, and Strommen C (1981). The entire compound autosomes of Drosophila melanogaster. Genetics 98, 257–273. 10.1093/genetics/98.2.257. [PubMed: 6799353]
53. Rong YS, Titen SW, Xie HB, Golic MM, Bastiani M, Bandyopadhyay P, Olivera BM, Brodsky M, Rubin GM, and Golic KG (2002). Targeted mutagenesis by homologous recombination in D. melanogaster. Genes Dev 16, 1568–1581. 10.1101/gad.986602. [PubMed: 12080094]
54. Karg T, Elting MW, Vicars H, Dumont S, and Sullivan W (2017). The chromokinesin Klp3a and microtubules facilitate acentric chromosome segregation. J Cell Biol 216, 1597–1608. 10.1083/jcb.201604079. [PubMed: 28500183]
55. Molitor TP, and Traktman P (2014). Depletion of the protein kinase VRK1 disrupts nuclear envelope morphology and leads to BAF retention on mitotic chromosomes. Mol Biol Cell 25, 891–903. 10.1091/mbc.E13-10-0603. [PubMed: 24430874]
56. Nichols RJ, Wiebe MS, and Traktman P (2006). The vaccinia-related kinases phosphorylate the N' terminus of BAF, regulating its interaction with DNA and its retention in the nucleus. Mol Biol Cell 17, 2451–2464. 10.1091/mbc.e05-12-1179. [PubMed: 16495336]
57. Samwer M, Schneider MWG, Hoefler R, Schmalhorst PS, Jude JG, Zuber J, and Gerlich DW (2017). DNA Cross-Bridging Shapes a Single Nucleus from a Set of Mitotic Chromosomes. Cell 170, 956–972 e923. 10.1016/j.cell.2017.07.038. [PubMed: 28841419]
58. Paumard-Rigal S, Zider A, Vaudin P, and Silber J (1998). Specific interactions between vestigial and scalloped are required to promote wing tissue proliferation in Drosophila melanogaster. Dev Genes Evol 208, 440–446. 10.1007/s004270050201. [PubMed: 9799424]

59. Siriaco GM, Cenci G, Haoudi A, Champion LE, Zhou C, Gatti M, and Mason JM (2002). Telomere elongation (Tel), a new mutation in Drosophila melanogaster that produces long telomeres. Genetics 160, 235–245. 10.1093/genetics/160.1.235. [PubMed: 11805059]
60. Mason JM, Frydrychova RC, and Biessmann H (2008). Drosophila telomeres: an exception providing new insights. Bioessays 30, 25–37. 10.1002/bies.20688. [PubMed: 18081009]
61. Hinton T, and Atwood KC (1941). Terminal Adhesions of Salivary Gland Chromosomes in Drosophila. Proc Natl Acad Sci U S A 27, 491–496. 10.1073/pnas.27.11.491. [PubMed: 16588490]
62. Rubin GM (1978). Isolation of a telomeric DNA sequence from Drosophila melanogaster. Cold Spring Harb Symp Quant Biol 42 *Pt* 2, 1041–1046. 10.1101/sqb.1978.042.01.104. [PubMed: 98261]
63. Karpen GH, and Spradling AC (1992). Analysis of subtelomeric heterochromatin in the Drosophila minichromosome Dp1187 by single P element insertional mutagenesis. Genetics 132, 737–753. 10.1093/genetics/132.3.737. [PubMed: 1334894]
64. Barefield C, and Karlseder J (2012). The BLM helicase contributes to telomere maintenance through processing of late-replicating intermediate structures. Nucleic Acids Res 40, 7358–7367. 10.1093/nar/gks407. [PubMed: 22576367]
65. Nera B, Huang HS, Lai T, and Xu L (2015). Elevated levels of TRF2 induce telomeric ultrafine anaphase bridges and rapid telomere deletions. Nat Commun 6, 10132. 10.1038/ncomms10132. [PubMed: 26640040]
66. d'Alcontres MS, Palacios JA, Mejias D, and Blasco MA (2014). TopoIIalpha prevents telomere fragility and formation of ultra thin DNA bridges during mitosis through TRF1-dependent binding to telomeres. Cell Cycle 13, 1463–1481. 10.4161/cc.28419. [PubMed: 24626180]
67. Chan KL, Palmai-Pallag T, Ying S, and Hickson ID (2009). Replication stress induces sister-chromatid bridging at fragile site loci in mitosis. Nat Cell Biol 11, 753–760. 10.1038/ncb1882. [PubMed: 19465922]
68. Hong Y, Velkova M, Silva N, Jagut M, Scheidt V, Labib K, Jantsch V, and Gartner A (2018). The conserved LEM-3/Ankle1 nuclease is involved in the combinatorial regulation of meiotic recombination repair and chromosome segregation in Caenorhabditis elegans. PLoS Genet 14, e1007453. 10.1371/journal.pgen.1007453. [PubMed: 29879106]
69. de Lange T (2009). How telomeres solve the end-protection problem. Science 326, 948–952. 10.1126/science.1170633. [PubMed: 19965504]
70. Kanda T, Otter M, and Wahl GM (2001). Mitotic segregation of viral and cellular acentric extrachromosomal molecules by chromosome tethering. J Cell Sci 114, 49–58. [PubMed: 11112689]
71. Kanda T, Sullivan KF, and Wahl GM (1998). Histone-GFP fusion protein enables sensitive analysis of chromosome dynamics in living mammalian cells. Curr Biol 8, 377–385. 10.1016/s0960-9822(98)70156-3. [PubMed: 9545195]
72. Gull K, Alsford S, and Ersfeld K (1998). Segregation of minichromosomes in trypanosomes: implications for mitotic mechanisms. Trends Microbiol 6, 319–323. 10.1016/s0966-842x(98)01314-6. [PubMed: 9746942]
73. Fuge H (1975). Anaphase transport of akinetochoric fragments in tipulid spermatocytes. Electron microscopic observations on fragment-spindle interactions. Chromosoma 52, 149–158. 10.1007/BF00326264. [PubMed: 1175461]
74. Sullivan W, Ashburner A, Hawley RS (2000). Drosophila Protocols (Cold Spring Harbor Laboratory Press).
75. Lin DM, and Goodman CS (1994). Ectopic and increased expression of Fasciclin II alters motoneuron growth cone guidance. Neuron 13, 507–523. 10.1016/0896-6273(94)90022-1. [PubMed: 7917288]
76. DeBruhl H, Wen H, and Lipsick JS (2013). The complex containing Drosophila Myb and RB/E2F2 regulates cytokinesis in a histone H2Av-dependent manner. Mol Cell Biol 33, 1809–1818. 10.1128/MCB.01401-12. [PubMed: 23438598]

77. Duan T, Kitzman SC, and Geyer PK (2020). Survival of Drosophila germline stem cells requires the chromatin-binding protein Barrier-to-autointegration factor. Development 147. 10.1242/dev.186171.

78. Golic KG (1994). Local transposition of P elements in Drosophila melanogaster and recombination between duplicated elements using a site-specific recombinase. Genetics 137, 551–563. 10.1093/genetics/137.2.551. [PubMed: 8070665]

79. Buffin E, Lefebvre C, Huang J, Gagou ME, and Karess RE (2005). Recruitment of Mad2 to the kinetochore requires the Rod/Zw10 complex. Curr Biol 15, 856–861. 10.1016/j.cub.2005.03.052. [PubMed: 15886105]

80. Warecki B, Bast I, and Sullivan W (2022). Visualizing the Dynamics of Cell Division by Live Imaging Drosophila Larval Brain Squashes. Methods Mol Biol 2415, 37–46. 10.1007/978-1-0716-1904-9_3. [PubMed: 34972944]

81. Wickham H (2016). ggplot2: Elegant Graphics for Data Analysis (Springer-Verlag).

Highlights

- DNA threads connect sister and non-sister telomeres in most early anaphases
- Telomere threads are normally resolved in mid-to-late anaphase
- Telomere threads recruit a set of proteins upon chromosome breakage
- Persistent protein-coated telomere threads promote retention of broken chromosomes

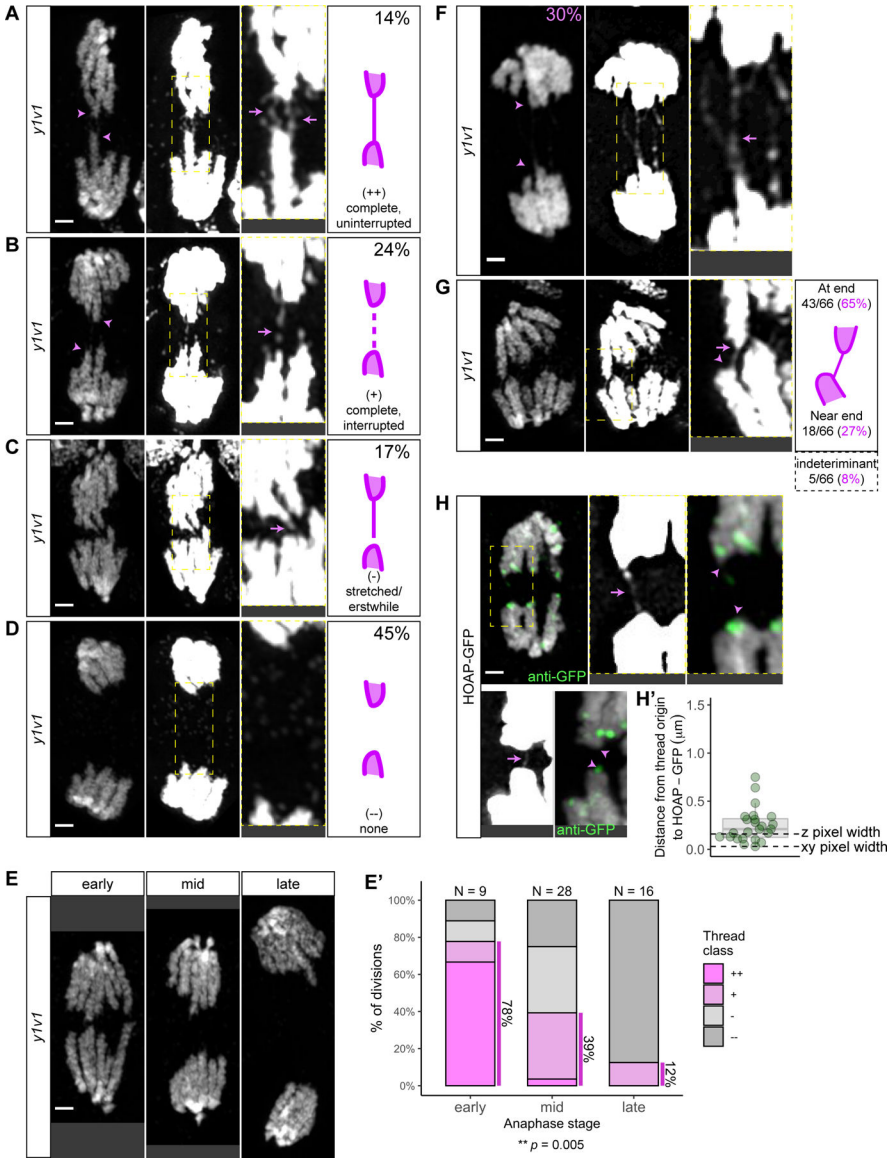

Figure 1. Anaphase chromosomes segregating to opposing poles remain connected by telomere-telomere DNA threads in normal divisions

For each image panel, left=unadjusted Airyscan max projection; middle=brightness/contrast enhanced; right=zoom of yellow boxed region. (A-D) Anaphase DAPI-stained *y1v1* neuroblasts showing representative examples of each thread class observed. Arrowheads indicate the connected ends. Arrows indicate threads. (A) Complete, uninterrupted (++) thread=DAPI signal with no gaps connecting chromosome ends. (B) Complete, interrupted (+) thread=DAPI signal with gaps connecting chromosome ends. (C) Stretched/erstwhile (−) thread=DAPI signal from only one chromosome end. (D) No thread (−−)=no DAPI signal. (E) Representative images of early, mid, and late anaphase neuroblasts (early=chromosome ends separated by < half the length of a chromosome arm, mid=chromosome ends separated by between half to twice the length of a chromosome arm, or late=chromosome ends separated by greater than twice the full length of a chromosome arm or chromosome arms are decondensed). (E') Comparison of the observed frequencies of thread classes

for early, mid, and late anaphase neuroblasts. (F) PI-stained anaphase *y1v1* neuroblast with a complete, interrupted (+) thread (arrow) connecting chromosome ends (arrowheads). (G) DAPI-stained *y1v1* anaphase neuroblast with a complete, uninterrupted (++) thread between one chromosome's end (arrow) and near the other chromosome's end (arrowhead). Quantification for the frequencies of thread origins at each location is also displayed. (H) Neuroblasts expressing the telomere capping protein HOAP-GFP fixed in anaphase. The origin points (arrowheads) of DAPI-stained threads (arrows) were generally from the location where HOAP was detected, although threads sometimes emerged from regions where we did not detect HOAP. (H') Quantification of the distance of thread origins from the nearest detected HOAP signal. Each dot represents one thread origin. Scale bars are 1 μm and 0.5 μm for unzoomed and zoomed images respectively. See also Figure S1.

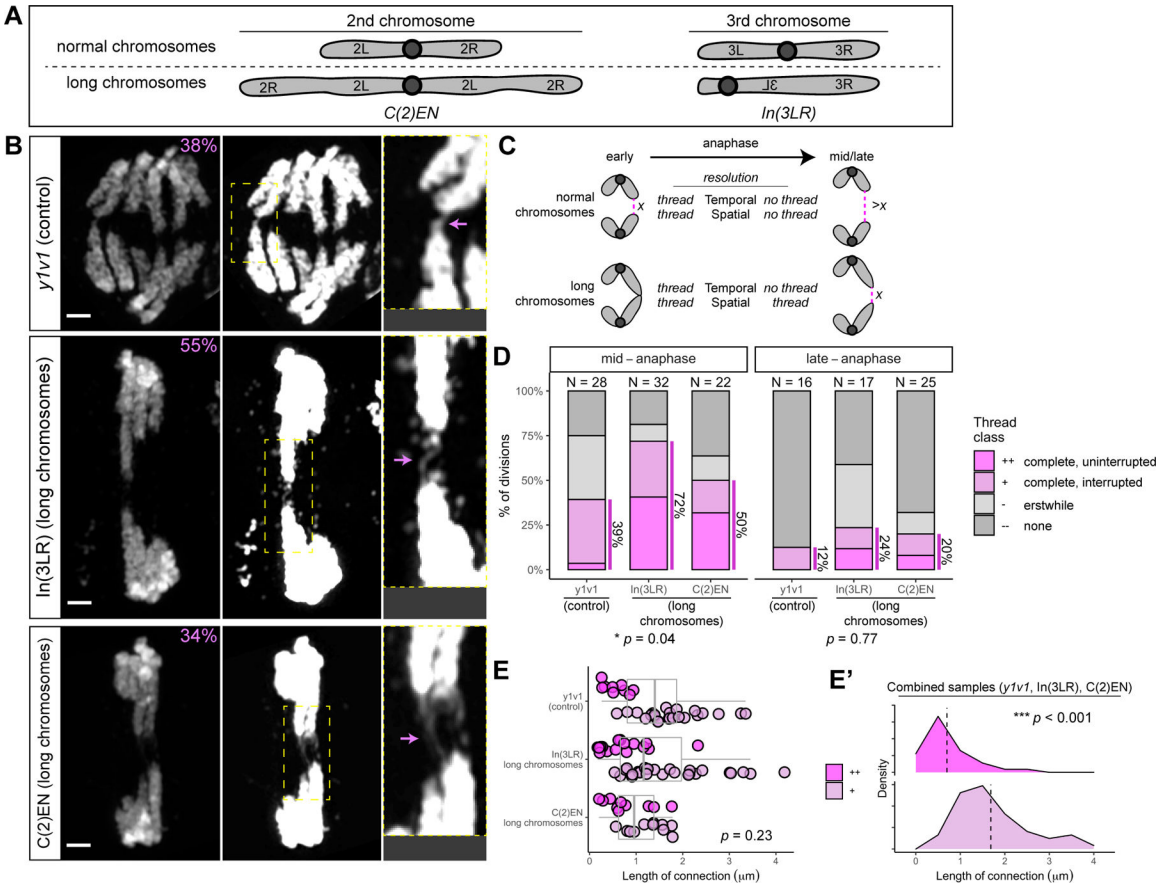

Figure 2. Inter-chromosomal DNA threads are primarily resolved by a spatial mechanism

For each image panel, left=unadjusted Airyscan max projection; middle=brightness/contrast enhanced; right=zoom of yellow boxed region. (A) The extra-long C(2)EN chromosome is made by combining both homologs of the 2nd chromosome onto one centromere. The extra-long In(3LR) chromosome is made by an inversion that places the centromere closer to one telomere, resulting in an elongated chromosome arm. (B) Anaphase DAPI-stained *y1v1* (top), In(3LR)-bearing (middle), and C(2)EN-bearing (bottom) neuroblasts showing representative examples of complete, uninterrupted (++) threads (arrows). Scale bars are 1 μm and 0.5 μm for unzoomed and zoomed images respectively. (C) In mid-to-late anaphase, a temporal resolution model predicts no threads would be observed in divisions with either normal-length or extra-long chromosomes. In contrast, a spatial resolution model predicts threads would be observed in mid-to-late anaphase divisions with extra-long chromosomes, because the distance between the extra-long chromatid ends (*X*) is comparable to the distance between the ends of normal-length chromatids earlier in anaphase. (D) Comparison of the observed frequencies of thread classes for *y1v1*, In(3LR)-bearing, and C(2)EN-bearing neuroblasts fixed in mid and late anaphase. (E) Comparison of the measured lengths of the observed threads for *y1v1*, In(3LR)-bearing, and C(2)EN-bearing neuroblasts. Each dot (magenta=++; pink=+) represents one thread color-coded for thread class. There is no significant difference in the measured lengths of threads between the control and extra-long chromosomes. (E') Density distributions of the combined measured thread lengths from (E)

for ++ (top) and + (bottom) threads, suggesting threads become stretched as chromosome ends move apart. See also Figure S2.

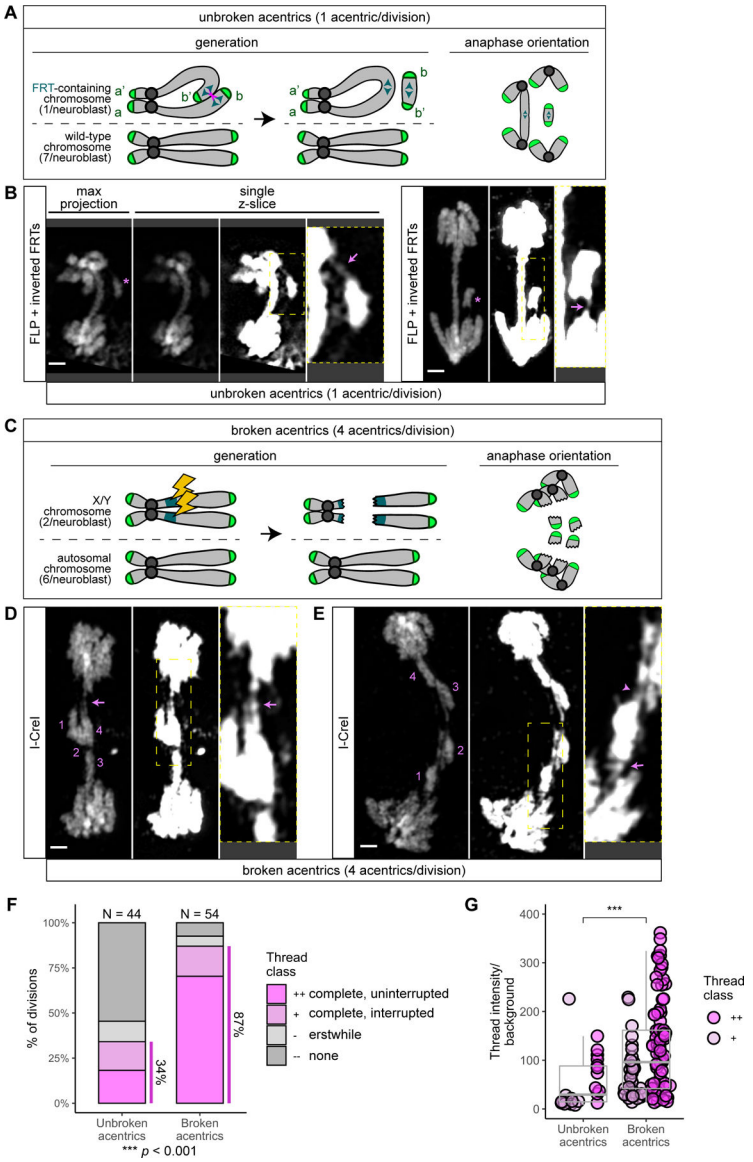

Figure 3. Lagging broken and unbroken acentrics are connected to segregating chromosomes by DNA threads

For each image panel, left=unadjusted Airyscan max projection; middle=brightness/contrast enhanced; right=zoom of yellow boxed region. (A) FLP-mediated recombination between sister chromatids bearing inverted FRTs (arrowheads) results in a dicentric chromosome and an unbroken acentric with intact telomeres. a and a' denote sister telomeres of the short arm. b and b' denote sister telomeres of the long arms. Sister telomeres are recombined onto the same DNA molecule. During anaphase, the acentric chromosome lags on the metaphase plate. (B) Two DAPI-stained FLP-expressing neuroblasts showing DNA threads (arrows) connecting unbroken acentrics (asterisks) to segregated chromosomes. For clarity, a single z-slice is shown for the neuroblast on the left. (C) I-CreI endonuclease recognizes its cut site (square) at the base of the X and Y chromosomes, resulting in an acentric fragment with a broken end and an intact telomere. During anaphase, the acentric chromosome fragment lags on the metaphase plate. (D-E) Anaphase DAPI-stained I-CreI-expressing neuroblasts

showing DNA threads connected to broken acentrics (labeled 1–4). Threads connect broken acentrics to segregating chromosomes (arrows) and to other acentrics (arrowhead). Some acentrics have threads emanating from both their ends (E). Scale bars are 1 μm and 0.5 μm for unzoomed and zoomed images respectively. (F) Comparison of the observed frequencies of thread classes connecting unbroken and broken acentrics. (G) Comparison of the normalized thread pixel intensity for threads connecting unbroken and broken acentrics. Each dot represents one thread. See also Figure S3.

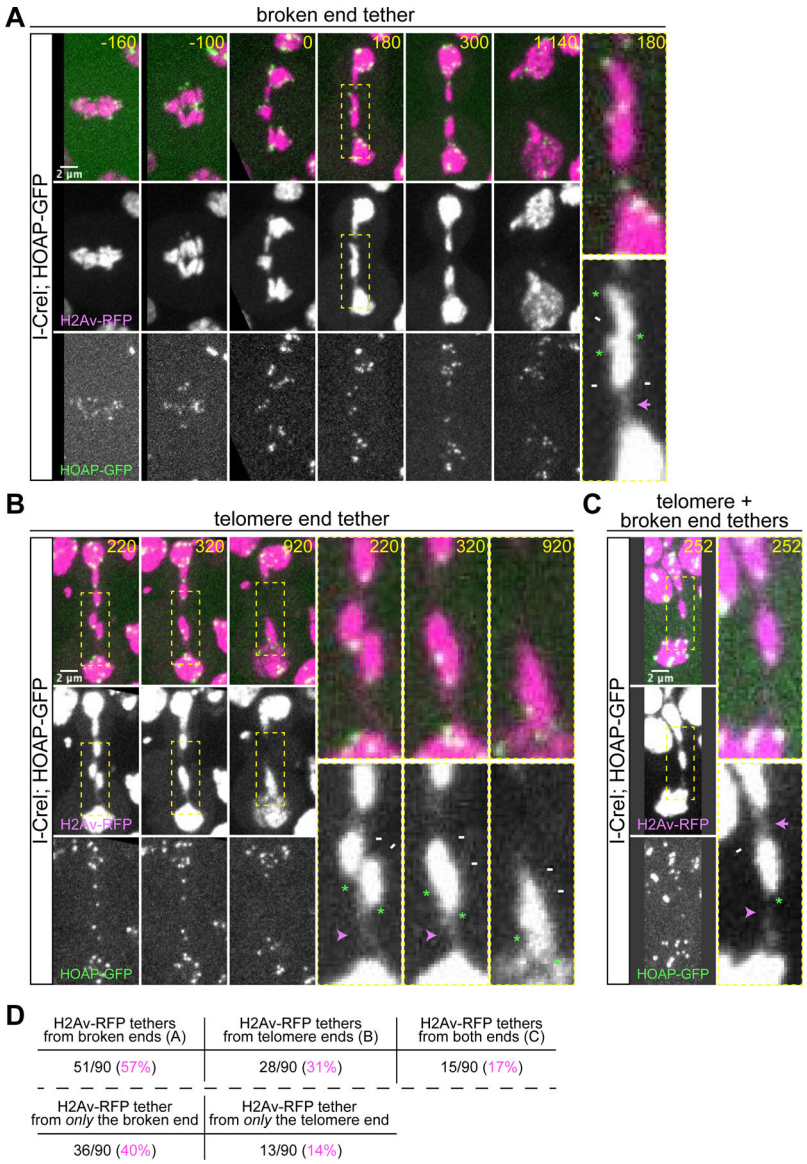

Figure 4. Histones are recruited to DNA threads emanating from the telomeres of broken acentrics

(A-C) Max projection stills from time lapse movies of neuroblasts expressing I-CreI, the chromosomal marker H2Av-RFP (magenta), and the telomere marker HOAP-GFP (green). (A) Histones are recruited to tethers (magenta arrows) that connect the broken ends (white arrows) of acentrics to segregating chromosomes [23]. See also Video S1. (B) Upon chromosome breakage, histones can also be recruited to the DNA threads (magenta arrowheads) emanating from the telomere ends (asterisks) of the acentrics. The histone-coated DNA thread in this cell connects non-sister telomeres. See also Video S2. (C) Some acentrics had histone-coated tethers originating from both their ends simultaneously. (D) Quantification of the frequencies of H2Av-RFP tethers emanating from broken, telomere, or both ends of individual acentrics. For each image panel, zoomed images of the merged and H2Av-RFP channels are shown for the yellow boxed region. Time is seconds before/after

acentric segregation. Scale bars are 2 μm and 1 μm for unzoomed and zoomed images respectively.

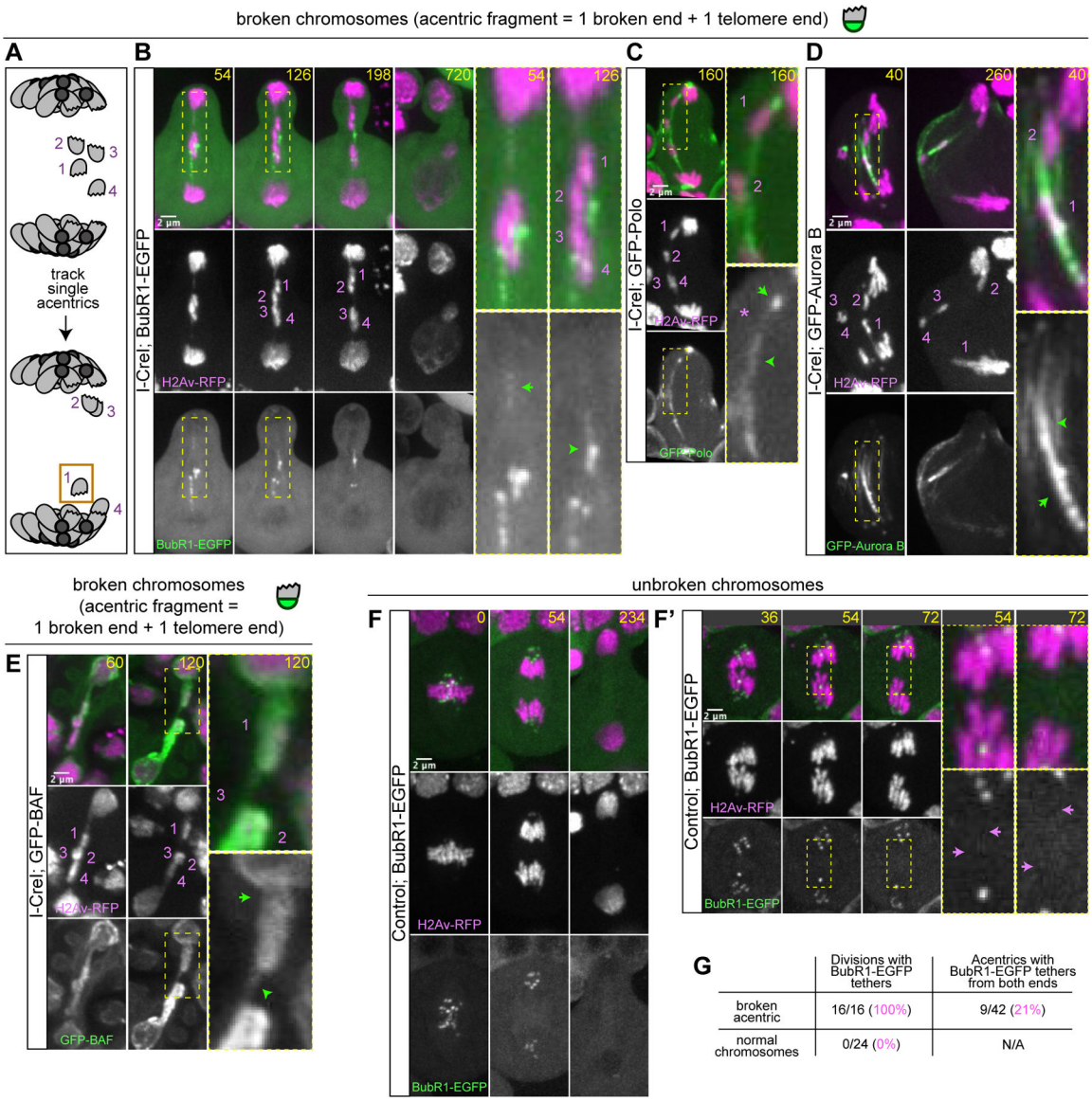

Figure 5. Telomere DNA threads recruit the tether proteins BubR1, Polo, Aurora B, and BAF upon chromosome breakage

(A) Expression of I-CreI in female larvae results in four broken X chromosome fragments. Single acentrics can be individually tracked through anaphase and assayed for the formation of protein-coated tethers simultaneously from both of their ends (broken and telomeric). (B-E) Max projection stills from time lapse movies of neuroblasts expressing I-CreI, H2Av-RFP (magenta), and either BubR1-EGFP (B, green; See also Video S3), GFP-Polo (C, green; See also Video S4), GFP-Aurora B (D, green; See also Video S5), or GFP-BAF (E, green; See also Video S6). BubR1, Polo, Aurora B, and BAF tethers can be observed connecting lagging acentrics to both segregating chromosomes (arrows) and to other acentrics (arrowheads). Each of the 4 individual acentrics in a division is marked by a number. Recruitment of these proteins to tethers off both ends of a single acentric simultaneously indicates their recruitment to the DNA thread emanating from the telomere end of the acentric. Time is seconds after acentric segregation. (F-F') Max projection stills

from time-lapse movies of neuroblasts expressing H2Av-RFP (magenta) and BubR1-EGFP (green). Neither BubR1 nor histones are detected coating telomere-telomere DNA threads in divisions without chromosome breaks, even in divisions when a chromosome is slightly lagging and its tip is directly opposed to its sister's tip (F', arrows). See also Video S7. Time is seconds before/after acentric segregation. Scale bars are 2 μm and 1 μm for unzoomed and zoomed images respectively. (G) Comparison of the frequency of observed BubR1-coated tethers between divisions in which I-CreI-induced broken chromosomes are present and normal divisions with unbroken chromosomes. For divisions with broken chromosomes, the overall frequency of BubR1-coated tethers and the frequency of acentrics with BubR1-coated tethers emanating from both ends is also compared. See also Figures S3 and S4.

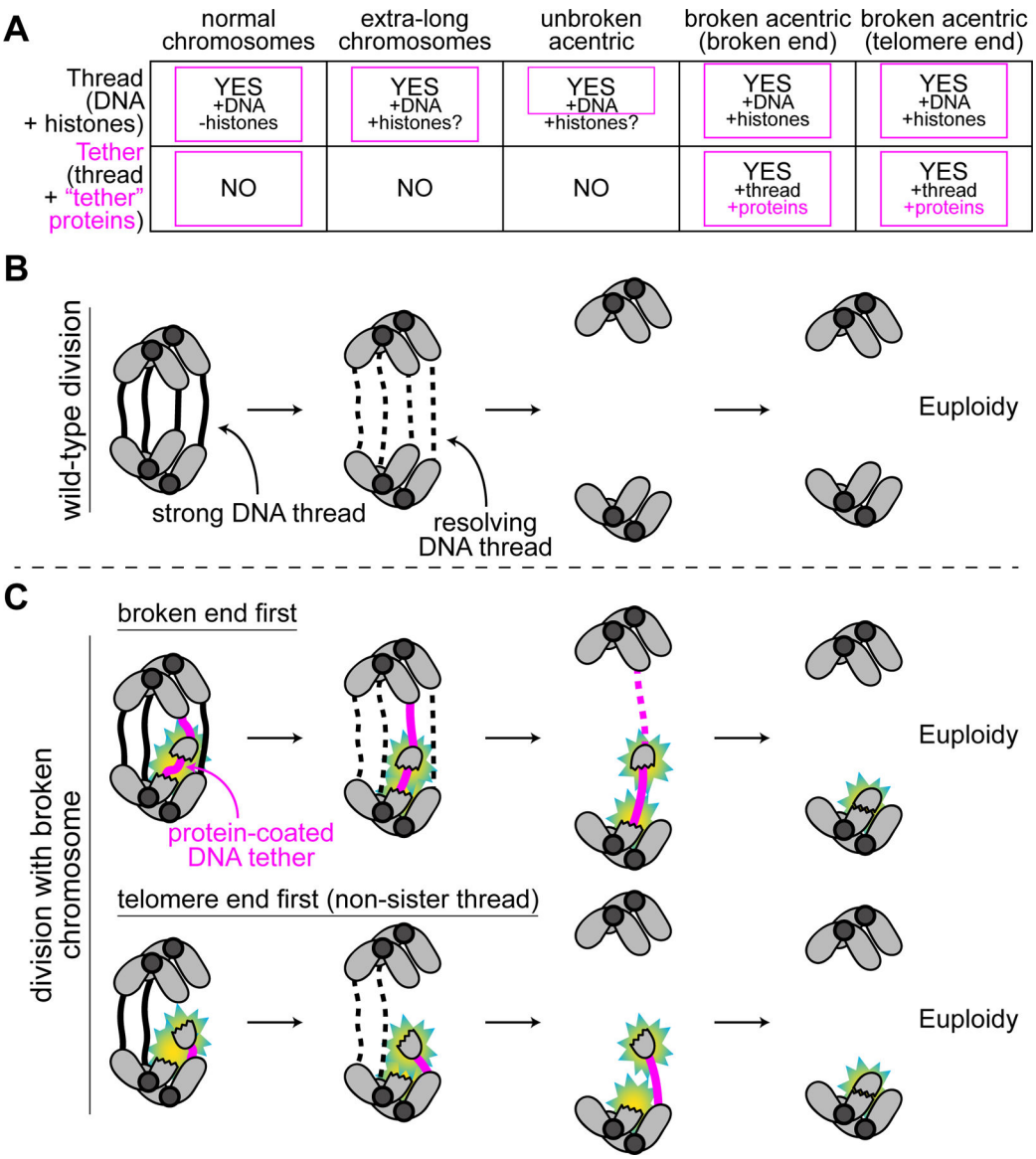

Figure 6. General telomere inter-chromosomal connections capture and retain lagging chromosomes to promote euploidy

(A) Summary of when threads (DNA + histones) and tethers (threads + proteins) connect anaphase chromosomes. Tethers/threads we directly observed are boxed. Question marks indicate histones were rarely detected. (B) In normal divisions, DNA threads connect the telomeres of most segregating sister chromatids. As the cell progresses through anaphase, threads stretch and are resolved, leading to complete genome separation and euploidy. (C) In divisions with broken chromosomes, broken ends (yellow-blue stars) produce a signal so that nearby telomere threads are coated with proteins (histones, BubR1, Polo, Aurora B, BAF) and stabilized to form tethers. This results in tethers from both the broken and telomere ends of acentrics (potentially connecting both sister and non-sister telomeres). Tethers persist in anaphase when threads are resolved and mediate segregation to the daughter nucleus. Thus, euploidy is efficiently maintained.

KEY RESOURCES TABLE

REAGENT or RESOURCE	SOURCE	IDENTIFIER
Antibodies		
chicken anti-GFP	Aves Lab	Cat# GFP-1010; RRID:AB_2307313
goat anti-chicken-Alexa488	Thermo Fisher Scientific	Cat# A-11039; RRID:AB_2534096
rabbit anti-LaminB1	Abcam	Cat# ab16048; RRID:AB_443298
goat anti-rabbit-Alexa488	Thermo Fisher Scientific	Cat# A-11008; RRID:AB_143165
Experimental Models: Cell Lines		
PC-3 cells	Gift from Wang Lab	RRID:CVCL_0035
Experimental Models: Organisms/Strains		
D. melanogaster: *y1v1*: y^1,v^1	Bloomington *Drosophila* Stock Center	RRID:BDSC_1509
D. melanogaster: In(3LR): In(3LR)264,mv^1/Tm6B,Tb^1	Bloomington *Drosophila* Stock Center	RRID:BDSC_1222
D. melanogaster: C(2)EN: C(2)EN,bw^1,$speck^1$	Bloomington *Drosophila* Stock Center	RRID:BDSC_1020
D. melanogaster: I-CreI: P{$v^{+t1.8}$=hs-I-CreI.R}2A,v^1;ry^{506}	Bloomington *Drosophila* Stock Center	RRID:BDSC_6936
D. melanogaster: BubR1-EGFP: w*;P{w^{+mC}=UAS-BubR1.EGFP}III.1	Bloomington *Drosophila* Stock Center	RRID:BDSC_91697
D. melanogaster: UAS-RpA-70 RNAi: y^1sc*$v^1$$sev^{21}$;P{$y^{+t7.7}$$v^{+t1.8}$=TRiP.GL00350}attP2	Bloomington *Drosophila* Stock Center	RRID:BDSC_35426
D. melanogaster: UAS-BubR1-DN: $y^1$$w^{1118}$;P{$w^{+mC}$=UAS-BubR1.DN}3	Bloomington *Drosophila* Stock Center, generated by Exelixis, Inc.	RRID:BDSC_8382
D. melanogaster: elav-Gal4: Elav-Gal4	Lin and Goodman[75]	N/A
D. melanogaster: GFP-Polo: Ubi-GFP-Polo	Gift from Lipsick Lab[76]	N/A
D. melanogaster: GFP-Aurora B: UAS-GFP-Aurora B	Gift from Lipsick Lab	N/A
D. melanogaster: I-CreI (III): w^{1118};P{$v^{+t1.8}$=hs-I-CreI.R}1A,Sb^1/Tm6	Gift from Golic Lab[53]	RRID:BDSC_6937
D. melanogaster: hs-FLP: w^{1118};P{$ry^{+t7.2+}$70FLP}10	Gift from Golic Lab[78]	RRID:BDSC_6938
D. melanogaster: inverted FRTs: P{FRT(w^{hs})}(8F)105	Gift from Golic Lab[78]	N/A
D. melanogaster: HOAP-GFP: w*;HOAP-GFP	Gift from Tamkun Lab	N/A
D. melanogaster: GFP-BubR1: w^{1118};GFP-BubR1	Buffin et al.[79]	N/A
D. melanogaster: GFP-Polo: w*;P{$w^{+mW.hs}$=GFP-polo}p2;P{GFP-polo}p31	Bloomington *Drosophila* Stock Center	RRID:BDSC_84275
D. melanogaster: GFP-BAF: y^1w*;GFP-BAF	Gift from Geyer Lab[77]	N/A
Software and Algorithms		
R	R Core Team	Version 4.0.5
ggplot2	Wickham[81]	Version 3.3.5
Other		

REAGENT or RESOURCE	SOURCE	IDENTIFIER
DAPI	Vector Laboratories	Cat# H-1200; RRID:AB_2336790